

1
2
3
4
5
6
7
8
9
10
11
12
13
14
15
16
17
18
19
20
21

Preprint of :

Villette, S., Piron, E., & Miclet, D. (2017). Hybrid centrifugal spreading model to study the fertiliser spatial distribution and its assessment using the transverse coefficient of variation. *Computers and Electronics in Agriculture*, 137, 115-129.
<http://doi.org/10.1016/j.compag.2017.03.023>

<http://www.sciencedirect.com/science/article/pii/S0168169917304325>

1 **Hybrid centrifugal spreading model to study the fertiliser spatial**
2 **distribution and its assessment using the transverse coefficient of variation**
3
4

5 S Villette ^{a,b*}, E Piron ^c, D Miclet ^c
6

7 ^a Agroécologie, AgroSup Dijon, INRA, Univ. Bourgogne Franche-Comté, F-21000 Dijon,
8 France

9 ^b Equipe Agroéquipements, AgroSup Dijon, BP 87999, 21079 Dijon Cedex, France

10 ^c IRSTEA, Les Palaquins, 03150 Montoldre, France
11

12 * Corresponding author.

13 E-mail address: sylvain.villette@agrosupdijon.fr
14

15 **Abstract**
16

17 Studying centrifugal spreading by carrying out field or in-door experiments using fertiliser
18 collection trays is tedious and labour intensive. This is particularly true when several
19 implementation methods need to be compared, numerous replications are required or fertiliser
20 sample characterisation is required. To circumvent cumbersome experiments, an alternative
21 approach consists in performing in silico studies. In order to reach this objective, a hybrid
22 centrifugal spreading model is designed by combining theoretical fertiliser motion equations
23 with statistical information. The use of experimental measurements to characterise fertiliser
24 properties, outlet velocity, angular mass flow distribution and spread pattern deposition,
25 ensure a realistic calibration of the model. Based on this model, static spread patterns and
26 transverse distributions are computed for a virtual twin-disc spreader. The number of fertiliser
27 granules used to compute a spread pattern is deduced from the target application rate while
28 the granule properties and their motion parameters are randomly selected from pre-established
29 statistical distributions. This Monte Carlo process reproduces the random variability of
30 fertiliser spread pattern depositions. Using this model, simulations demonstrate the mean and
31 standard deviation of CV value decrease with the application rate. The CV mean value also
32 decreases with the collection tray surface, while the standard deviation decreases with the
33 collection tray length. Mathematical relationships are deduced from simulation results to
34 express the mean and standard deviation of the CV as functions of the application rate and
35 collection tray surface or length. The simulation model is also used to compare spreader test
36 methods and study the influence of some fertiliser particles properties on the transverse
37 distribution.
38
39

40 **Keywords**
41

42 Centrifugal spreading, Coefficient of Variation, Model, Monte Carlo, Simulation, Virtual
43 spreader
44
45
46

1	Notation	
2		
3	a	regression parameter
4	A_p	particle frontal area, m^2
5	b	regression parameter
6	c	regression parameter
7	C_d	drag coefficient
8	CV	transverse coefficient of variation, %
9	CV_{geom}	geometrical component of the CV, %
10	CV_k	value of the CV obtained when the collection tray width is w_k , %
11	D	continuous random variable, m
12	d_p	fertiliser granule diameter, m
13	d_{pi}	diameter of the i^{th} fertiliser granule, m
14	$F_D(d_p)$	cumulative frequency function of the granule diameter
15	$f_D(d_p)$	probability density function of the granule diameter
16	g	acceleration due to gravity, $m\ s^{-2}$
17	$G_D(d_p)$	cumulative mass distribution function of the granule diameter
18	$G_M(\theta_{vane})$	cumulative mass flow distribution with respect to the vane location
19	$g_M(\theta_{vane})$	mass flow distribution with respect to the vane location
20	h_{vane}	height of the outer extremity of the vane, m
21	K	constant, m^3
22	K_a	aerodynamic coefficient, m^{-1}
23	l_{tray}	length of the collection tray, m
24	L_w	swath spacing, m
25	m	particle mass, kg
26	$m(d_p)$	mass of a granule of diameter d_p , kg
27	m_i	mass of the i^{th} fertiliser granule, kg
28	m_{tot}	total mass of fertiliser ejected by the two discs of the virtual spreader, kg
29	n_{disc}	number of granules ejected by one disc of the virtual spreader
30	(O, i, j, k)	Cartesian frame centred on the disc centre, with j oriented in the travel direction
31		
32	q_t	target application rate, kg/ha
33	q_f	in-field target rate, kg/ha
34	r	Pearson correlation coefficient
35	r_{vane}	radius of the vane, m
36	s_{disc}	distance between the two disc axles of the virtual spreader, m
37	t	time, s
38	v_H	horizontal component of the outlet velocity, $m\ s^{-1}$
39	v_{out}	outlet velocity, $m\ s^{-1}$
40	(v_x, v_y, v_z)	velocity components of the granule during the ballistic flight, m
41	$(v_{xout}, v_{yout}, v_{zout})$	components of the outlet velocity, $m\ s^{-1}$
42	w_k	width of the collection trays
43	(x, y, z)	coordinates of the granule, m
44	$(x_{out}, y_{out}, z_{out})$	coordinates of the granule when it leaves the vane, m
45	α_{lv}	pitch angle of the vane, $^\circ$
46	α_{set}	setting angle of the virtual spreader, $^\circ$
47	Δl_{grid}	grid sampling interval along the travel direction, m
48	Δw_{grid}	grid sampling interval along the transverse direction, m
49	θ_{out}	horizontal outlet angle of the granule when it leaves the vane, $^\circ$
50	θ_{raj}	horizontal orientation of the outlet velocity with respect to i , $^\circ$

1	θ_{vane}	angular location of the vane with respect to i , °
2	μ_{CV}	mean value of the CV, %
3	μ_{ln}	fitting parameter of the cumulative mass distribution
4	$\mu\theta_{out}$	mean value of the horizontal outlet angle, °
5	ξ	variable of integration, m
6	ρ	density of the fertiliser granule, kg m ⁻³
7	ρ_{air}	air density, kg m ⁻³
8	$\sigma\theta_{out}$	standard deviation of the horizontal outlet angle, °
9	$\sigma\Omega_{out}$	standard deviation of the vertical outlet angle, °
10	σ_{CV}	standard deviation of CV, %
11	σ_{ln}	fitting parameter of the cumulative mass distribution
12	ω	rotational speed of the spinning disc, rad s ⁻¹
13	Ω_{out}	vertical outlet angle of the granule, °
14	Ω_{vane}	vertical angle of the vane, °
15		
16		
17		

1 1. Introduction

2
3 In agriculture, the objective of mineral fertiliser supplies is to provide the right rate of
4 nutrients to cultivated plants. Because of their low cost and high productivity, centrifugal
5 spreaders are widely used for this application aiming to spread fertiliser at a target rate with
6 an acceptable uniformity in the field. For 50 years several works have demonstrated the
7 negative effects of non-uniform spatial distributions concerning environmental impacts
8 ([Tissot et al., 2002](#)) and yield or economical losses ([Horrell et al., 1999](#); [Jensen and Pesek,](#)
9 [1962](#); [Miller et al., 2009](#); [Richards and Hobson, 2013](#); [Søgaard and Kierkegaard, 1994](#); [Tissot](#)
10 [et al., 1999](#)). For the same decades, numerous works have been devoted to the measurement
11 of fertiliser distributions, the assessment of distribution quality and the understanding of
12 spread patterns. Throughout the world, transverse tray tests are traditionally performed to
13 measure the spreading uniformity according to various standards such as: [ISO Standard](#)
14 [5690/1 \(1985\)](#); [ASAE Standards S341.2 \(1999\)](#); [EN 13739-2 \(2003\)](#); Spreadmark code of
15 practice ([New Zealand Fertiliser Quality Council \(2015\)](#)) or ACCU Spread ([Australian](#)
16 [Fertiliser Services Association, 2001](#)). The experimental transverse distribution is then used to
17 compute the coefficient of variation CV after overlapping. This CV value is used to quantify
18 the spreading quality, define the appropriate swath spacing according to the fertiliser and the
19 spreader setting, and thus certify the spreader bout width.

20 Some studies have addressed the comparison of transverse distribution measurement methods.
21 Several works investigated the influence of the collection systems. [Parish \(1986\)](#) compared
22 twelve collection methods in laboratory conditions using a manually-operated rotary spreader
23 and two granular materials. The maximal effective swath width of this spreader was 4.3 m.
24 Each test run consisted of three passes and three replications where carried out. Using the
25 results obtained in this previous work, [Parish and de Visser \(1989\)](#) analysed the effect of the
26 collection tray width on the CV value. In field, [Parish et al. \(1987\)](#) compared the crop
27 response quality assessed by a horticulturist with the fertiliser rates deduced from transverse
28 distribution measurements. Three collection methods were compared using three replications
29 for each test. All these studies demonstrated that, depending on the test method, major
30 differences occurred in the measurement of the transverse distribution. Therefore, the authors
31 highlighted the importance of using the same test method for comparisons of spreader
32 performance. Moreover regarding the low throwing distance of the spreader chosen for these
33 studies and the low number of replications, these works illustrate the difficulties of carrying
34 out such experiments.

35 To perform statistical comparisons of six international spreader tests, [Jones et al. \(2008\)](#)
36 carried out a huge experimental work by using 18 transverse rows of 80 trays each. The
37 experiments were carried out with urea, for three application rates and two replications so that
38 36 transverse distributions were obtained for each spreading situation. The bout width of the
39 spreader was 15 m. Concerning the prediction of the certifiable working width, the authors
40 concluded that the ACCU Spread test method ([Australian Fertiliser Services Association,](#)
41 [2001](#)) was superior to the other tested standards because it uses two rows of collector trays
42 and multiple passes. [Jones et al. \(2008\)](#) concluded multiple rows of trays, multiple passes of
43 the spreader and long trays can improve the accuracy of transverse tests.

44 Since the transverse distribution results from the combination of numerous parameters, it only
45 provides a limited piece of information concerning the spread pattern. Thus, transverse tests
46 are not efficient to study how mechanical parameters or fertiliser characteristics affect the 2D
47 spread pattern deposition. This was illustrated by [Piron and Miclet \(2005\)](#) who showed that
48 different 2D static spread patterns can yield to similar transverse patterns. Unfortunately, the
49 measurement of the 2D static spread pattern is very tedious when a grid of collection trays is
50 used, because of the wide size of spreader footprints and the high number of trays required to

1 cover this area. Moreover, for indoor test, the high throwing distance of recent spreaders
2 would require very expensive infrastructures. To circumvent these difficulties, [Piron and](#)
3 [Miclet \(2005\)](#) developed a rotating test bench called CEMIB. With this method, the spreader
4 is rotated during the spreading and a radial row of collection trays equipped with load cells
5 records the cumulated mass of fertiliser according to the angular orientation of the spreader.
6 The static spread pattern is then derived from the cumulated mass and the CV of the
7 transverse distribution can be deduced ([EN 13739-2, 2011](#)). The measurement of the 2D
8 spread pattern is of particular interest to improve the understanding of the spread pattern
9 formation, the understanding of mechanical parameter effects and more generally to design
10 new spreader. It is also useful to calibrate or validate spreading models.

11 Recently, [Cool et al. \(2015\)](#) addressed the design of a simplified measurement technique to
12 estimate the 2D static spread pattern in field, using a limited number of collection trays placed
13 on a square or polar grid. The results of these two sampling techniques were compared with
14 the results obtained with a transverse test. Tests were carried out with a spreader whose
15 setting corresponded to 15 m bout width for ammonium nitrate fertiliser. Tests were
16 performed for three fertilisers without replication. The authors observed large differences in
17 the CV values deduced from the three measurement techniques and highlighted the
18 importance of using the same measurement techniques to compare spread patterns. As this
19 kind of experiments is tedious and does not make possible a sufficient number of replications
20 to compare significant values, this work illustrates the need of alternative approaches when
21 the design or the assessment of new spreading quality measurement techniques is required.

22
23 The complexity and the labour-intensive nature of experimental measurements further
24 increase when the study is not limited to the fertiliser mass distribution but aims to analyse the
25 size or the nutrient formulation of the granules with respect to their spatial distribution. For
26 example, very few studies investigated the effect of fertiliser particle size on spread
27 distribution. [Pettersen et al. \(1991\)](#) studied the spatial distribution of fertiliser particle size
28 using a twin disc spreader. Experiments were limited to the choice of one fertiliser, one
29 spreader setting, one feeding flow rate and one measurement of the 2D stationary spread
30 pattern. A set of 884 collected samples was analysed by image processing technique to draw
31 the spatial distribution of the particle size. Thirty years later, [Yule \(2011\)](#) attempted to study
32 the effect of fertiliser particle size on spread distribution. The transverse distribution of the
33 percentage of particle size was drawn for two loads of superphosphate having different
34 granule size distributions. [Yule \(2011\)](#) used these experimental results to simulate the
35 transverse distribution of other materials with other particle size characteristics. Nevertheless,
36 the author underlined the work is limited to representing only one particular spreading
37 situation: one spreader with one fertiliser and one setting. [Yule \(2011\)](#) concluded that further
38 work would be required but analysing each tray from field testing was too time-consuming
39 and no laboratory measurement techniques were adapted for this kind of study at the present
40 time.

41 The study of the spatial distribution of fertiliser granules according to their physical properties
42 is of particular interest in the case of blended fertilisers. As these materials are produced by
43 mixing mechanically single products, their components differ in the physical properties (size,
44 shape and density). These differences can involve segregation of the fertiliser components
45 during handling and spreading. This problem was already addressed by [Hoffmeister et al.](#)
46 [\(1964\)](#). When fertiliser is applied with a centrifugal spreader, the differences in physical
47 properties can affect the granule behaviour during the ballistic flight. Then, ballistic
48 segregation can occur and yield heterogeneous spatial distribution of chemical elements.
49 Several works have examined the ballistic segregation of blended fertilisers by carrying out

1 field experiments ([Miserque and Pirard, 2004](#); [Tissot et al., 1999](#); [Virk et al., 2013](#)). All these
2 studies required huge field test to evaluate the mass and nutrient distribution.
3 In order to circumvent cumbersome experiments or reduce the number of experiments, some
4 author attempted to develop new approaches based on modeling fertiliser granule motion.
5 Recently, [Antille et al. \(2013\)](#) suggested the particle size range of new fertilisers could be
6 designed to meet a target bout width and the author proposed to model and simulate the
7 ballistic flight to assess whether granule physical properties suited the spreading objective.
8 [Grafton et al. \(2015\)](#) also suggested the use of a ballistic model to provide information to
9 reduce the risk of crop striping. In these recent works, the proposed models were limited to
10 predict the landing distance of some individual granules projected by a spinning disc.
11 Therefore, no spread pattern was computed so that no transverse distribution can be
12 determined.

13
14 Numerous works have attempted to model the motion of fertiliser granules in the spreading
15 process. Various mechanical models have been proposed to describe the motion of individual
16 fertiliser granules on a spinner disc ([Cunningham, 1963](#); [Cunningham and Chao, 1967](#);
17 [Hofstee, 1995](#); [Inns and Reece, 1962](#); [Olieslagers, 1997](#); [Patterson and Reece, 1962](#); [Villette
18 et al., 2005](#)) and through the air ([Antille et al., 2015](#); [Mennel and Reece, 1963](#); [Pitt et al.,
19 1982](#)). Concerning the motion on the disc, models using the discrete element method (DEM)
20 have also been developed to take into account particle interactions ([Casas et al., 2015](#);
21 [Coetzee and Lombard, 2011](#); [Tijskens et al., 2005](#); [Van Liedekerke et al., 2006](#)). One
22 drawback of DEM models is that they required input parameters that are difficult to obtain to
23 characterise the physical behaviour of fertilisers. When results of simulations are compared
24 with actual spread pattern depositions, they reach moderate success even when spreading
25 distances are lower than 3m ([Coetzee and Lombard, 2011](#); [Van Liedekerke et al., 2009](#)).
26 Consequently, at the present time, no model appears sufficiently advanced to correctly
27 simulate actual spread pattern depositions. Moreover, to the best of our knowledge, no model
28 reproduces the random variability observed from run to run in spreader test.

29
30 Despite some experimental studies, the comparison of spreader transverse tests using different
31 collection trays or different test protocols is still difficult and the main conclusion is limited to
32 the recommendation of using the same test to give sense to comparisons. For example, there is
33 a lack of knowledge concerning the quantitative effect of the surface or shape of collection
34 trays on the CV measurement. Similarly, the effect on the CV of increasing the number of
35 runs or reducing the speed travel of some standard tests has not been studied. In addition, the
36 effect of the application rate on the measurement of the CV value has never been studied. This
37 lack of information results from the difficulty, not to say impossibility, of carrying out
38 adapted experiments with enough replications. The same difficulty limited the production of
39 knowledge on the spatial distribution of fertiliser particle size and on the ballistic segregation
40 for blended fertilisers. An alternative solution lies in the use of models to simulate the
41 physical phenomena and carry out in silico experimental studies. The main advantages of this
42 approach are to avoid practical and time limitations so that statistical parameters can be
43 deduced from replications. Nevertheless, this implies that simulation models have to
44 reproduce the stochastic nature of fertiliser dispersal processes.

45 The aim of this paper is to design such a model for simulating realistic fertiliser spread
46 patterns and providing new solutions to carry out numerical experiments. This hybrid model
47 combines a mechanistic approach based on the use of mechanical relationships and a
48 stochastic approach based on the use of the statistical distributions of input parameters. The
49 simulation model is used to study the sense of the CV value deduced from transverse tests
50 according to the target application rate and the test method. The paper also presents an insight

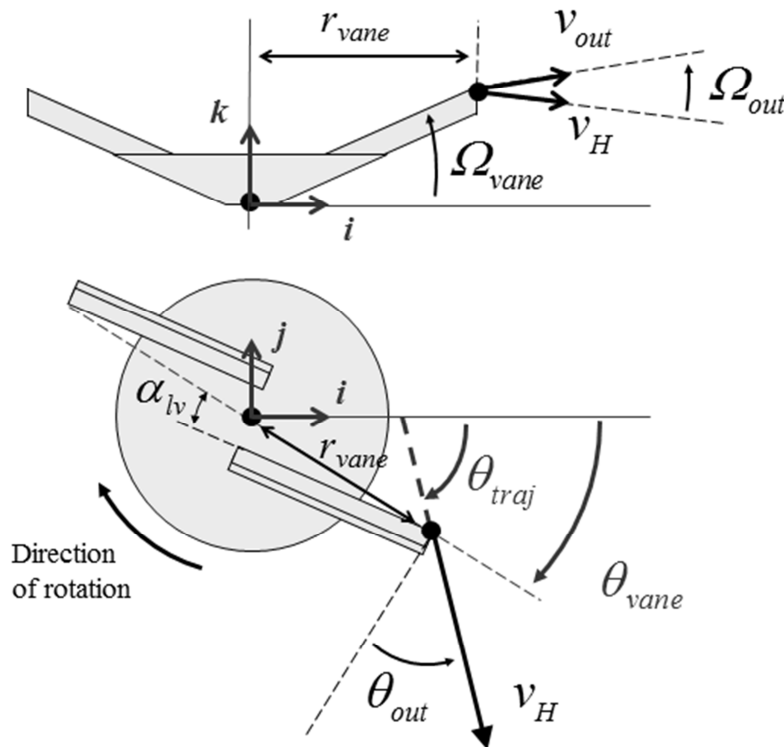
1 into the influence of particle size distributions and particle drag coefficients on transverse
 2 distributions.

3 4 5 **2. Materials and methods**

6
7 The particularity of the Hybrid Centrifugal Spreading Model HCSM lies in combining some
 8 theoretical motion models with experimental data obtained at various steps of the spreading
 9 process. This model assumes the spread pattern deposition is affected by the outlet velocity of
 10 the particles when they leave the spinning disc, the angular mass flow distribution around the
 11 disc and the fertiliser particle properties (specific density, size-distribution, drag coefficient).
 12

13 **2.1 Model of granule motion on and off the spinning disc**

14
15 Concerning the motion of the granules on the spinning disc, the HCSM considers the
 16 kinematic relationships between the disc configuration, the outlet angles and the outlet
 17 velocity components. In this section, the motion model is described for a clockwise spinning
 18 disc. Figure 1 presents the main geometrical parameters used to describe the disc and the
 19 motion of the granules when they leave the vane.



20
21 Fig. 1 - Side view (top) and top view (bottom) of a clockwise spinning disc: v_{out} , outlet
 22 velocity; v_H , horizontal component of the outlet velocity; θ_{out} , horizontal outlet angle; θ_{traj} ,
 23 horizontal angle of the trajectory; Ω_{out} , vertical outlet angle; r_{vane} , radius of the vane; α_{lv} , pitch
 24 angle of the vane; i, j, k , vectors of a right handed Cartesian coordinate system centred on the
 25 disc axle.

26
27 Let (O, i, j, k) be a three dimensional right-handed Cartesian coordinate system having its
 28 origin O on the rotational axle of the disc and with j pointing in the travel direction.

29 In this coordinate system, the location $(x_{out}, y_{out}, z_{out})$ of the granule when it leaves the vane is:

$$\begin{cases} x_{out} = r_{vane} \times \cos \theta_{vane} \\ y_{out} = r_{vane} \times \sin \theta_{vane} \\ z_{out} = h_{vane} \end{cases} \quad (1)$$

where r_{vane} is the radius of the vane, θ_{vane} is the angular location of the vane, h_{vane} is the height of the outer extremity of the vane.

For a concave disc, the relationship between the vertical outlet angle Ω_{out} of the particle when it leaves the vane, the horizontal outlet angle θ_{out} , the vertical angle of the vane Ω_{vane} and the pitch angle of the vane α_{lv} , is as follows:

$$\Omega_{out} = \arctan \left(\frac{\sin \theta_{out} \tan \Omega_{vane}}{\cos \alpha_{lv}} \right) \quad (2)$$

The horizontal component of the outlet velocity is also deduced from θ_{out} as follows:

$$v_H = \frac{r_{vane} \omega}{\cos \theta_{out} + \sin \theta_{out} \tan \alpha_{lv}} \quad (3)$$

where ω is the rotational speed of the disc.

Demonstrations of equations (2) and (3) can be found in [Villette et al. \(2008\)](#).

Then, the outlet velocity is deduced:

$$v_{out} = \frac{v_H}{\cos \Omega_{out}} \quad (4)$$

According to Fig. 1, for a clockwise rotating disc, the expression of the horizontal orientation θ_{traj} of the outlet velocity with respect to \mathbf{i} is as follows:

$$\theta_{traj} = \theta_{vane} + \theta_{out} - 90^\circ \quad (5)$$

The components of the outlet velocity in the Cartesian coordinate system (O, \mathbf{i} , \mathbf{j} , \mathbf{k}) are:

$$\begin{cases} vx_{out} = v_H \times \cos \theta_{traj} \\ vy_{out} = v_H \times \sin \theta_{traj} \\ vz_{out} = v_{out} \times \sin \Omega_{out} \end{cases} \quad (6)$$

In this model, owing to Eq. (2), the vertical outlet angle is not taken as the vertical angle of the vane unlike some other models suggested in the literature ([Gomez-Gil et al., 2009](#); [Olieslagers et al., 1996](#)). This avoids coarse approximations in computing the initial conditions of the ballistic flight.

During the ballistic flight the model considers that the forces acting on the granule are only the gravity force and the drag force due to the motion of the granule through immobile air. This simple ballistic model had been used in numerous works such as [Mennel and Reece \(1963\)](#), [Pitt et al. \(1982\)](#), [Griffis et al. \(1983\)](#), [Olieslagers et al. \(1996\)](#), [Grift and Hofstee \(2002\)](#), [Reumers et al. \(2003\)](#), [Aphale et al. \(2003\)](#), [Bradley and Farnish \(2005\)](#). In the three dimensional Cartesian coordinate system, the motion in the air is described by the following differential equations:

$$\begin{cases} \frac{d^2x}{dt^2} = -K_a vx \sqrt{vx^2 + vy^2 + vz^2} \\ \frac{d^2y}{dt^2} = -K_a vy \sqrt{vx^2 + vy^2 + vz^2} \\ \frac{d^2z}{dt^2} = -g - K_a vz \sqrt{vx^2 + vy^2 + vz^2} \end{cases} \quad (7)$$

1 where x, y, z are the coordinates of the granule; v_x, v_y, v_z are the velocity components of the
2 granule, g is the acceleration due to gravity and K_a is as follows:

$$3 \quad K_a = \frac{1}{2m} C_d A_p \rho_{air} \quad (8)$$

4 where m is the granule mass, C_d is the drag coefficient, A_p is the projected surface area of the
5 granule, ρ_{air} is the air density. In this study, A_p is computed for spherical shapes.

6 7 **2.2 Spreading process parameters**

8
9 The HCSM uses experimental data measured at the beginning and at the end of the ballistic
10 flight. This provides the initial parameters of the ballistic flight (i.e. outlet velocity) but also
11 makes possible the estimation of the drag coefficient during the flight. The combination of
12 these experimental measurements with mechanical models is of particular interest to take into
13 account the actual behaviour of the fertiliser in the spreading process ([Grift et al., 2006](#);
14 [Reumers et al., 2003](#)) and to provide realistic simulations.

15 In the spreading simulations, the motion of a high number of fertiliser granules is computed.
16 To compute one simulation some variables are taken constant for all granules while some
17 other variables assign random values for each granule. These last variables are associated with
18 certain probability distributions. Thus, some probability distribution functions or the
19 corresponding cumulative distribution functions needs to be defined.

20 This section describes the input parameters used in the simulations and their measurement
21 methods.

22 23 2.2.1 Experimental spreading device and spread pattern deposition

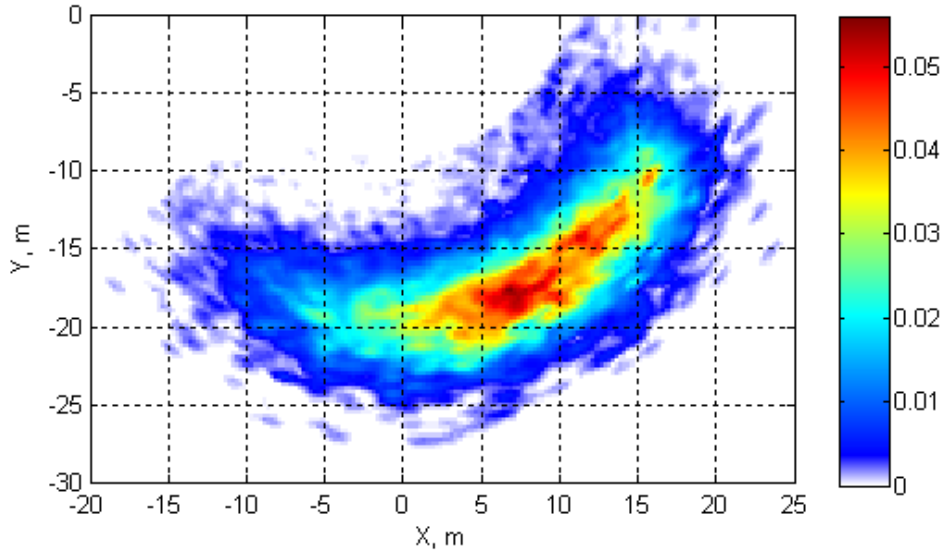
24
25 A custom-made spreader was used for the experimental measurements. This spreader
26 consisted of a single clockwise rotating disc. This concave disc was equipped with two radial
27 vanes (Ω_{vane} was 13.5° ; α_{iv} was 0° ; r_{vane} was 0.395 m) and was spinning at 810 rpm. The
28 height h_{vane} of the outer extremity of the vanes was 0.8 m. The feeding mass flow was 0.97
29 kg/s.

30 The stationary spread pattern obtained with this spreader and with ammonium nitrate was
31 measured using a rotating test bench called CEMIB. This measurement device consisted in a
32 rotating carrier and a motionless line of 80 collection trays. Each tray was equipped of a load
33 cell and had a square collection area of 0.5×0.5 m. The design and the advantages of this test
34 bench are detailed in [Piron and Miclet \(2005\)](#) and [Piron et al. \(2010\)](#).

35 During the spreading, the spreader carrier turned at a constant rotation speed of $3.1^\circ/s$, so that
36 the whole spread pattern passed above the collection tray row. During the rotation, the
37 cumulated mass collected by each tray was recorded and the weight values were stored with
38 the corresponding orientation angle of the carrier, measured by an angular optical encoder.
39 The acquisition frequency was 10 Hz. During the whole carrier rotation, the total fertiliser
40 mass ejected by the spreader was approximately 38 kg and the total mass collected by all the
41 trays was approximately 0.45 kg.

42 Using this measurement device, the resulting raw data was a matrix where each line
43 corresponded to an orientation angle and each column corresponded to the cumulative
44 fertiliser mass collected in each tray. The fertiliser mass collected at each angular location was
45 then derived from cumulative measurements. Since the collection areas of all trays are the
46 same, the spatial density of the fertiliser deposition was directly deduced from previous data
47 in polar coordinates. Then, the spread pattern deposition was computed by the CEMIB
48 algorithm, with respect to the disc centre in Cartesian coordinates, using a mathematical
49 interpolation and a sampling interval of 0.25×0.25 m. Figure 2 presents the spread pattern

1 deposition obtained with the experimental spreader and the ammonium nitrate fertiliser used
 2 in this study. This spread pattern is taken as reference data for the study.
 3 The analysis of the spread pattern deposition shows that the mean radius of the spread pattern
 4 slightly increases with the rotation of the vane (i.e. from the beginning to the end of the
 5 spreading angular sector).



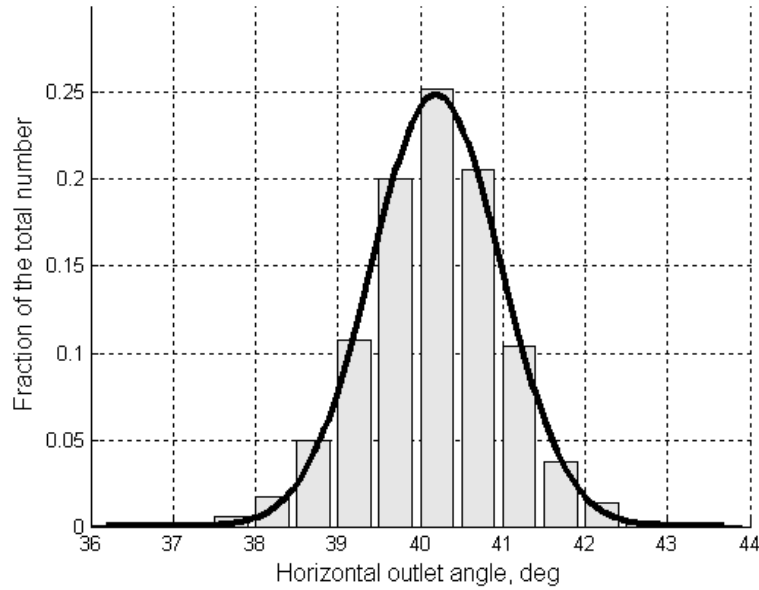
6
 7 Fig. 2 - Stationary spread pattern obtained for ammonium nitrate and the experimental
 8 spreader. The graduation of the colour scale reflects the fertiliser amount lying on the
 9 sampling area (0.25×0.25 m) expressed in percentage of the total mass.

10
 11 2.2.2 Horizontal outlet angle distribution

12
 13 The horizontal outlet angles θ_{out} were measured using an imaging system based on the
 14 processing of motion-blurred images. In this acquisition technique, the exposure time is long
 15 relative to the velocity of fertiliser granules so that the granule displacements appear as
 16 streaks across the image. The horizontal outlet angles were derived from the distance between
 17 these streaks and the disc axle. The imaging system and the image processing are detailed in
 18 [Villette et al. \(2008\)](#).

19 Images were captured with a monochrome CCD camera (Sony XCD-SX910), equipped with a
 20 6 mm lens. The camera was approximately placed at 0.7 m above the upper corner of the vane
 21 and approximately above the central part of the spreading angular sector. The optical axis of
 22 the camera was set parallel to the disc axle at a distance of approximately 0.5 m from this
 23 axle. Using a set of 300 images, the horizontal outlet angle was measured for trajectories
 24 selected near the principal point of the image (i.e. the point corresponding to the view axis in
 25 the image) to improve the measurement accuracy and avoid geometrical bias. Thus, 2280
 26 trajectories lying in a 10° spreading angular sector were used to estimate the horizontal outlet
 27 angle. The angular location of the vane θ_{vane} corresponding to the middle of this sector was -
 28 20° . The mean value $\mu_{\theta_{out}}$ was 40.2° and the standard deviation $\sigma_{\theta_{out}}$ was 0.85° .

29 Considering the histogram of the measured value (Fig. 3), the probability density function was
 30 chosen as a normal distribution defined by the two parameters: $\mu_{\theta_{out}}$ and $\sigma_{\theta_{out}}$.



1
2 Fig. 3 - Distribution histogram of the horizontal outlet angle measured in the middle of the
3 spreading angular sector. The Gaussian curve that fits the distribution is superposed
4 (continuous line).

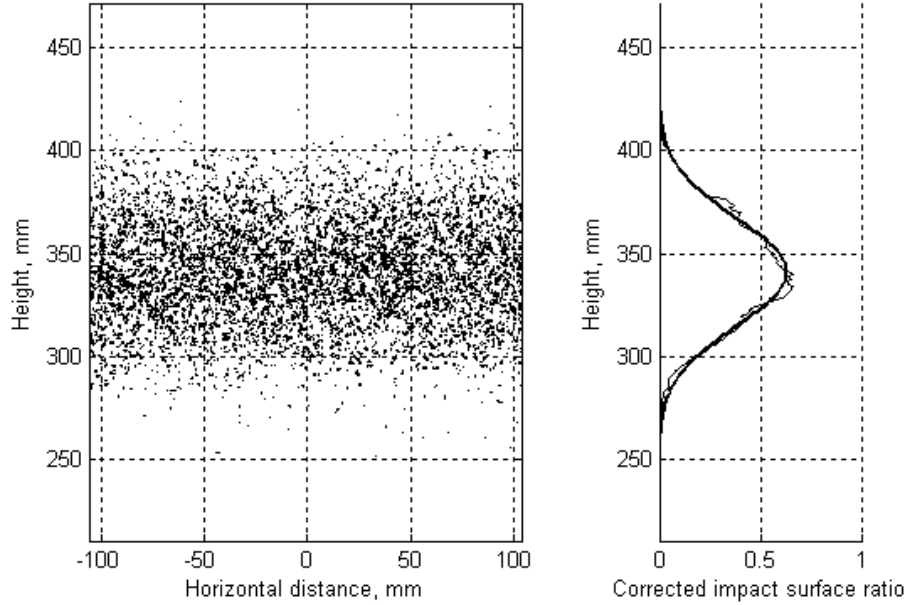
5
6 In order to take into account, the slight increase of the spread pattern radius with respect to the
7 rotation of the vane, the mean value $\mu\theta_{out}$ was modelled by the following linear relationship:

$$8 \quad \mu\theta_{out} = 39.2 - 0.05 \times \theta_{vane} \quad (9)$$

9 where $\mu\theta_{out}$ and θ_{vane} are expressed in degrees.

10 11 2.2.3 Vertical outlet angle distribution

12
13 For a given value of the horizontal outlet angle θ_{out} , the mean value of the corresponding
14 vertical outlet angle Ω_{out} was provided by Eq. (2). Nevertheless, this relationship did not
15 model the dispersion of Ω_{out} around its mean value. Consequently this dispersion was
16 measured separately by analysing the vertical distribution of the mass flow. The experimental
17 method consisted in recording granule impacts on a vertical screen placed in the vicinity of
18 the spinning disc. The method is the same than the one described in [Villette et al. \(2013\)](#),
19 except a simple flat screen was used instead of a cylindrical screen. Moreover a shutter
20 system was added to control the exposure time of the screen to fertiliser impacts. The screen
21 was covered with a paper of A4 size, a carbon film and a protective film, so that granules
22 hitting the screen produced impact marks on the recording paper (Fig. 4). After the exposition
23 of the recording paper to granule shocks, the paper was digitalised and a dedicated image
24 processing was carried out to analyse the vertical distribution of the impacts. The details of
25 the mathematical model and algorithms used to process impact records or compute the
26 corrected impact surface ratio, can be found in [Villette et al. \(2013\)](#). Considering the curve of
27 the vertical distribution of the impacts (Fig. 4), the probability density function was chosen as
28 a normal distribution. Placing the recording screen at 1.08 m and 2.09 m from the axle of the
29 spinning disc, 5 replications of impact recording were carried out at each distance. The mean
30 values of the standard deviations of the impact heights were respectively: 13.3 mm and 25.9
31 mm. Then, the standard deviation $\sigma\Omega_{out}$ of the vertical outlet angle was estimated at 0.7°.



1
2 Fig. 4 - Example of impact record (left) and the corresponding vertical impact distribution
3 (right) expressed in terms of corrected impact surface ratio. The Gaussian curve (bold) that
4 fits the distribution is superposed.

5 6 2.2.4 Angular mass flow distribution

7
8 The angular mass flow distribution was computed at the outer extremity of the vane, as a
9 function of the angular location of the vane. The distribution was deduced from the spread
10 pattern deposition and the horizontal outlet angle. The whole spreading angular sector was
11 sampled each degree. For each angular location of the vane, the theoretical horizontal
12 direction was computed using Eq. (5) and the relative fertiliser quantity was computed for
13 each sampled angular sector from the outer extremity of the vane to a range of 30 m with a
14 sampling interval of 0.25 m. Thus, the spread pattern deposition was computed as a function
15 of the spreading distance (from the extremity of the vane to the landing point) and the angular
16 location of the vane (Fig. 5). The angular mass flow distribution $g_M(\theta_{vane})$ at the extremity of
17 the vane (Fig. 5) was obtained by summing the relative mass of fertiliser obtained for each
18 vane location (whatever the spreading distance). The cumulative mass flow distribution with
19 respect to the vane location $G_M(\theta_{vane})$ was deduced from $g_M(\theta_{vane})$ as follows:

$$20 \quad G_M(\theta_{vane}) = \int_{-\infty}^{\theta_{vane}} g_M(\xi) d\xi \quad (10)$$

21 This distribution was used in the HCSM to compute the probability of the fertiliser mass
22 ejected for each angular position of the vane for the clockwise spinning disc of the virtual
23 spreader.
24

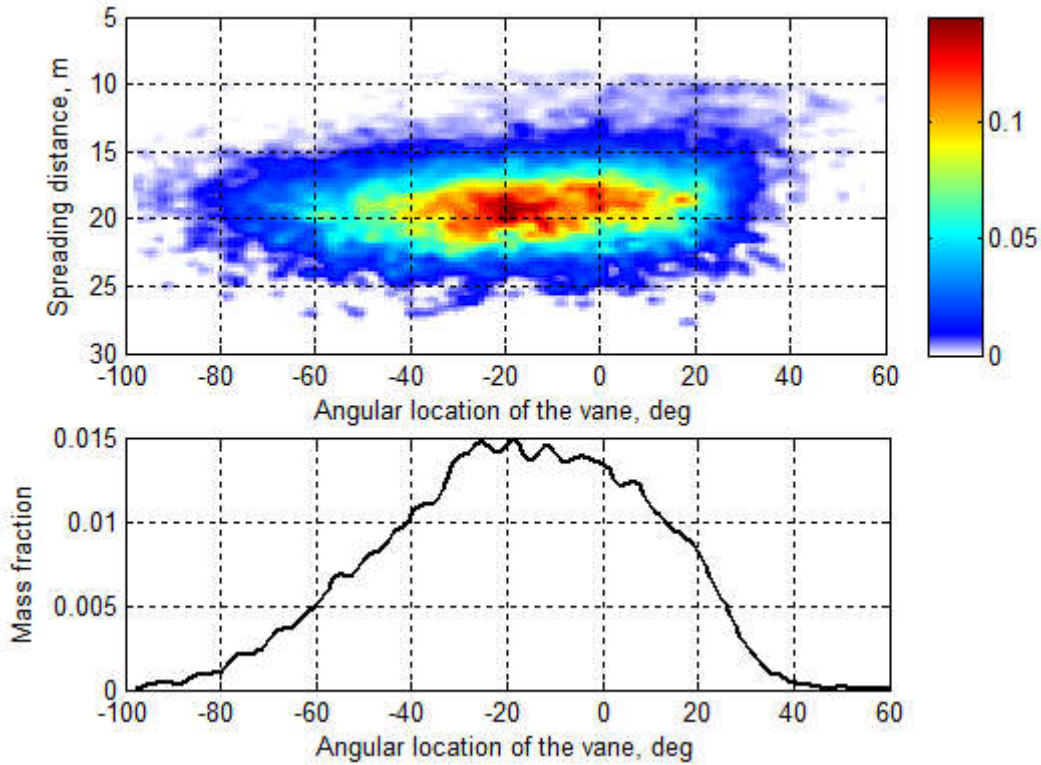


Fig. 5 - Spread pattern deposition (top) and angular distribution of the mass flow (bottom). The spread pattern deposition is drawn as a function of the spreading distance and the angular location of the vane. The graduation of the colour scale reflects the fertiliser amount lying on the sampling area ($0.25 \text{ m} \times 1^\circ$), expressed in percentage of the total mass.

2.3 Fertiliser parameters

In this study, ammonium nitrate was used for actual experiments. The same fertiliser characteristics were used in numerical simulations computed with the HSCM. The shape of the granules was assumed to be spherical.

2.3.1 Specific density

The density of the fertiliser granules was deduced from weighing a material bulk volume and weighing anew the same bulk volume after completing with a liquid of known density. Then, the volume of the granules is deduced and the granule density is calculated. For the ammonium nitrate used in this study, the specific density ρ was 1563 kg.m^{-3} .

2.3.2 Granule diameter distribution

The particle size analysis was performed with a sieving test according to the European standard EN 1235/A1 (2003). This provided the cumulative mass distribution function. Then, a two-parameter lognormal distribution was used to describe the distribution.

Thus, the normalised cumulative mass distribution (value range from 0 to 1) was fit with the following function:

$$G_D(d_p) = \frac{1}{2} + \frac{1}{2} \operatorname{erf} \left(\frac{\ln(d_p) - \mu_{ln}}{\sqrt{2}\sigma_{ln}} \right) \quad (11)$$

1 where d_p is the granule diameter, erf() is the error function, μ_m and σ_m are the two fitting
 2 parameters (corresponding to the mean and standard deviation of the variable's natural
 3 logarithm).

4 The derivative function of $G_D(d_p)$ is:

$$5 \quad g_D(d_p) = \frac{1}{d_p \sigma_m \sqrt{2\pi}} \exp\left(-\frac{(\ln(d_p) - \mu_m)^2}{2\sigma_m^2}\right) \quad (12)$$

6 Considering the probability density function $f_D(d_p)$ and the cumulative frequency function
 7 $F_D(d_p)$ of the random variable D , the probability of having the granule diameter D lower than
 8 d_p is:

$$9 \quad p(\{D \leq d_p\}) = F_D(d_p) = \int_0^{d_p} f_D(\xi) d\xi \quad (13)$$

10 Using the probability density function $f_D(d_p)$, the cumulative mass distribution $G_D(d_p)$ is also
 11 expressed as follows:

$$12 \quad G_D(d_p) = \frac{\int_0^{d_p} f_D(\xi) \times m(\xi) d\xi}{\int_0^{+\infty} f_D(\xi) \times m(\xi) d\xi} \quad (14)$$

13 where $m(d_p)$ is the mass of granules of diameter d_p .

14 Assuming the mass of the granule is proportional to d_p^3 , Eq. (14) yields:

$$15 \quad G_D(d_p) = \frac{1}{K} \int_0^{d_p} f_D(\xi) \times \xi^3 d\xi \quad (15)$$

16 where $K = \int_0^{+\infty} f_D(\xi) \times \xi^3 d\xi$

17 This provides:

$$18 \quad g_D(d_p) = \frac{1}{K} f_D(d_p) \times d_p^3 \quad (16)$$

19 Combining Eq. (13) and Eq. (16), the cumulative frequency function of the granule diameter
 20 is finally obtained as follows:

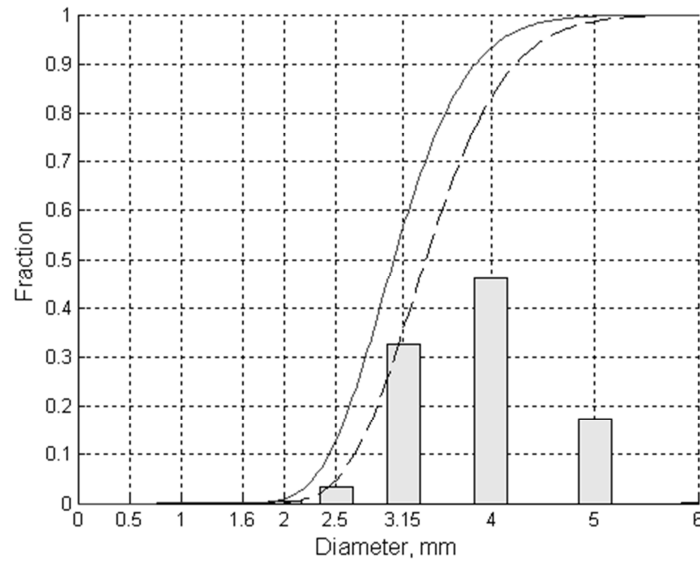
$$21 \quad F_D(d_p) = K \int_0^{d_p} \frac{g_D(\xi)}{\xi^3} d\xi \quad (17)$$

22 In practice, the integration of Eq. (17) is computed numerically and the constant K is
 23 determined so that $F_D(d_p)$ is 1 when d_p tends to infinity.

24

25 For the ammonium nitrate fertiliser used in this study, Fig. 6 presents the results of the sieve
 26 test with the corresponding cumulative mass distribution $G_D(d_p)$ and the cumulative frequency
 27 function $F_D(d_p)$.

28



1
2 Fig. 6 - Results of the particle size analysis: fraction of the fertiliser mass retained on each
3 sieve (bar graph), cumulative mass distribution $G_D(d_p)$ (dashed line), cumulative frequency
4 function $F_D(d_p)$ (continuous line).

5
6 The establishment of the cumulative frequency function $F_D(d_p)$ is of particular interest to
7 select efficiently random diameter values corresponding to a random set of granules whose
8 the mass distribution respects the fertiliser sieve test.

9 10 2.3.3 Drag coefficient in the air

11
12 To compute the ballistic flight of fertiliser particles, many researchers assumed the drag
13 coefficient C_d to be constant ([Coetzee and Lombard, 2011](#); [Grafton et al., 2015](#); [Grift and](#)
14 [Hofstee, 2002](#); [Olieslagers et al., 1996](#); [Pitt et al., 1982](#)), while some other authors tried to
15 improve the description of the ballistic flight by considering changes of the C_d value during
16 the motion ([Antille et al., 2015](#)).

17 In some works, the fertiliser particles were approximated as perfect spheres. Consequently,
18 considering a turbulent flow regime, the C_d value of the fertiliser granules was chosen at 0.44
19 ([Coetzee and Lombard, 2011](#); [Olieslagers et al., 1996](#); [Walker et al., 1997](#)). Taking into
20 account the influence of shape and texture of fertiliser granules on their aerodynamic
21 behaviour, some other authors chose higher C_d values. For instance, [Pitt et al. \(1982\)](#) chose
22 0.46 for ammonium nitrate. Comparing modelled and measured fall time, [Grift and Hofstee](#)
23 [\(2002\)](#) suggested multiplying the diameter of the equivalent sphere by a correction factor
24 (named “q-factor”) ranged from 0 to 1.

25 In the present study, the drag coefficient was assumed constant during the ballistic flight. The
26 value of C_d was chosen by comparing the reference spread pattern (i.e. obtained with the
27 CEMIB test bench) with simulated spread patterns computed for various C_d values. Thus, for
28 the ammonium nitrate used in this study, the value of the drag coefficient was estimated to
29 0.47. Moreover, the air density ρ_{air} was assumed to be 1.21 kg/m^3 in the spreading condition.

30 31 **2.4 Monte Carlo Spreading Simulation**

32 33 2.4.1 The virtual spreader

34
35 The virtual spreader considered for the simulations was a twin disc spreader for which the
36 spacing between the two disc axles s_{disc} was 1 m. Both discs had the same angular speed. The

1 right disc rotated in the counter-clockwise direction while the left one rotated in the clockwise
 2 direction. Each disc of the spreader was fed by the same mass flow of fertiliser.
 3 The setting of the virtual spreader consisted in modifying the angular location of the feeding
 4 point on each disc. With this setting mechanism, rotating the angular location of α_{set} for the
 5 left disc involves the rotation of the left spread pattern in the same direction and with the same
 6 angle α_{set} .

8 2.4.2 Static spread pattern simulation

10 Considering the virtual spreader, static spread patterns were computed using the HCSM and a
 11 Monte Carlo process. This approach consisted in computing the motion of a high number of
 12 fertiliser granules for which several characteristics were randomly drawn from pre-established
 13 statistical distributions. Simulations were implemented with [Matlab \(2005\)](#), and used the
 14 random number generator of this software. For normally distributed variables, the values were
 15 obtained using the *randn* function. In the case of other arbitrary distributions, the selection of
 16 random values was performed in two steps. First, random numbers were generated with a
 17 uniform distribution using the *rand* function on the range 0 to 1. Second, final random values
 18 were deduced from these random numbers by inverting the cumulative frequency function of
 19 the specified distribution.

20 For a given mass m_{tot} of fertiliser, the computation of the spread pattern was decomposed in
 21 computing the left and the right spread patterns independently. For the left disc, the Monte
 22 Carlo simulation consisted of the following steps.

24 First, a set of virtual granules was generated by drawing a set of diameter values from the
 25 fertiliser diameter distribution using the cumulative frequency function F_D . Then, the mass m_i
 26 of each granule was computed as follows:

$$27 \quad m_i = \rho \frac{\pi}{3} d_{pi}^3 \quad (18)$$

28 where d_{pi} is the diameter of the granule of mass m_i .

29 The total number n_{disc} of granules ejected by the disc was adjusted so that:

$$30 \quad \sum_{i=1}^{n_{disc}} m_i = \frac{m_{tot}}{2} \quad (19)$$

32 Second, the initial conditions of the ballistic flight were assigned to each granule
 33 independently from its diameter. For each granule, the values of the different variables were
 34 assigned as follows:

35 1) The angular location of the vane θ_{vane} corresponding to the granule ejection was randomly
 36 selected using the cumulative mass flow distribution G_D .

37 2) The corresponding coordinates of the ejection point $(x_{out}, y_{out}, z_{out})$ were deduced from θ_{vane}
 38 using Eq. (1).

39 3) The corresponding horizontal outlet angle θ_{out} was drawn from the normal distribution
 40 parametrized by $\mu_{\theta_{out}}$ and $\sigma_{\theta_{out}}$, where $\mu_{\theta_{out}}$ was deduced from the vane location θ_{vane} using
 41 Eq. (9).

42 4) The corresponding vertical outlet angle Ω_{out} was drawn from the normal distribution
 43 parametrized by $\mu_{\Omega_{out}}$ and $\sigma_{\Omega_{out}}$, where $\mu_{\Omega_{out}}$ was the vertical outlet angle deduced from θ_{out}
 44 using Eq. (2).

45 5) The corresponding outlet velocity v_{out} and its 3D-components $(v_{x_{out}}, v_{y_{out}}, v_{z_{out}})$ were
 46 deduced from θ_{vane} , θ_{out} and Ω_{out} using successively Eqs. (3), (4), (5) and (6).

1 Third, the coordinates of the landing point of each granule were computed by solving Eq. (7)
2 with the initial conditions of flight x_{out} , y_{out} , z_{out} and v_{xout} , v_{yout} , v_{zout} . Then, the setting of the
3 spreader is taken into account by computing the coordinates of the landing points with the
4 rotation angle α_{set} around the disc axle.

5
6 The spread pattern produced by the right disc is computed by 1) using anew the same process
7 to generate a second spread pattern for another set of granules; 2) changing the sign of the x
8 coordinates of this second spread pattern.

9 The global spread pattern resulting from the twin-disc virtual spreader is finally deduced from
10 the left and right spread patterns after translating the coordinates of the granules by half the
11 disc spacing s_{disc} in the left or right direction. This global spread pattern is defined by a set of
12 granules for which each mass and each landing position is perfectly known.

13 14 2.4.3 Transverse distribution

15
16 The transverse distribution is deduced from the static spread pattern by considering a virtual
17 row of collection trays placed continuously along a line perpendicular to the travel axis (along
18 the x -axis) of the virtual spreader. For a given swath spacing L_w , several static spread patterns
19 were computed and translated on the right and the left at a multiple of L_w of the central pass to
20 reproduce the overlapping. The successive spread patterns were oriented to simulate overlaps
21 resulting from adjacent swaths applied in alternate directions (*i.e.* back and forth mode).

22 Depending on the x -value of each granule of the spread patterns, the granules were affected to
23 the corresponding collection trays, so that the sub-set of granules virtually collected by each
24 tray was perfectly known in terms of granule masses and granule diameters. The transverse
25 distribution of the fertiliser mass was obtained by summing the mass of all the granules
26 virtually collected by each collection tray. Then, the transverse coefficient of variation CV is
27 deduced from this mass distribution by dividing the standard deviation by the mean. In this
28 paper the CV is expressed in percentage.

29 For a target application rate q_t , the total mass m_{tot} of fertiliser used to compute the static
30 spread pattern was determined as the product of the application rate by the collection surface
31 on the swath spacing. Calling l_{tray} the length of the collection trays (measured in the travel
32 direction), the total mass m_{tot} is as follows:

$$33 \quad m_{tot} = q_t \times l_{tray} \times L_w \times 10^{-4} \quad (20)$$

34 35 3 Results and discussion

36 37 **3.1 Comparison of the measured and simulated spread pattern**

38
39 Although the objective of the HCSM was not the perfect description of the physical
40 phenomena of the spreading process or the perfect reproduction of the experimental spread
41 pattern, it is important to ensure the simulated spread pattern was in accordance with
42 experimental results. Thus, the first simulation consisted in computing the spread pattern for a
43 single disc for the same spreading conditions than those carried out with the experimental
44 spreading device.

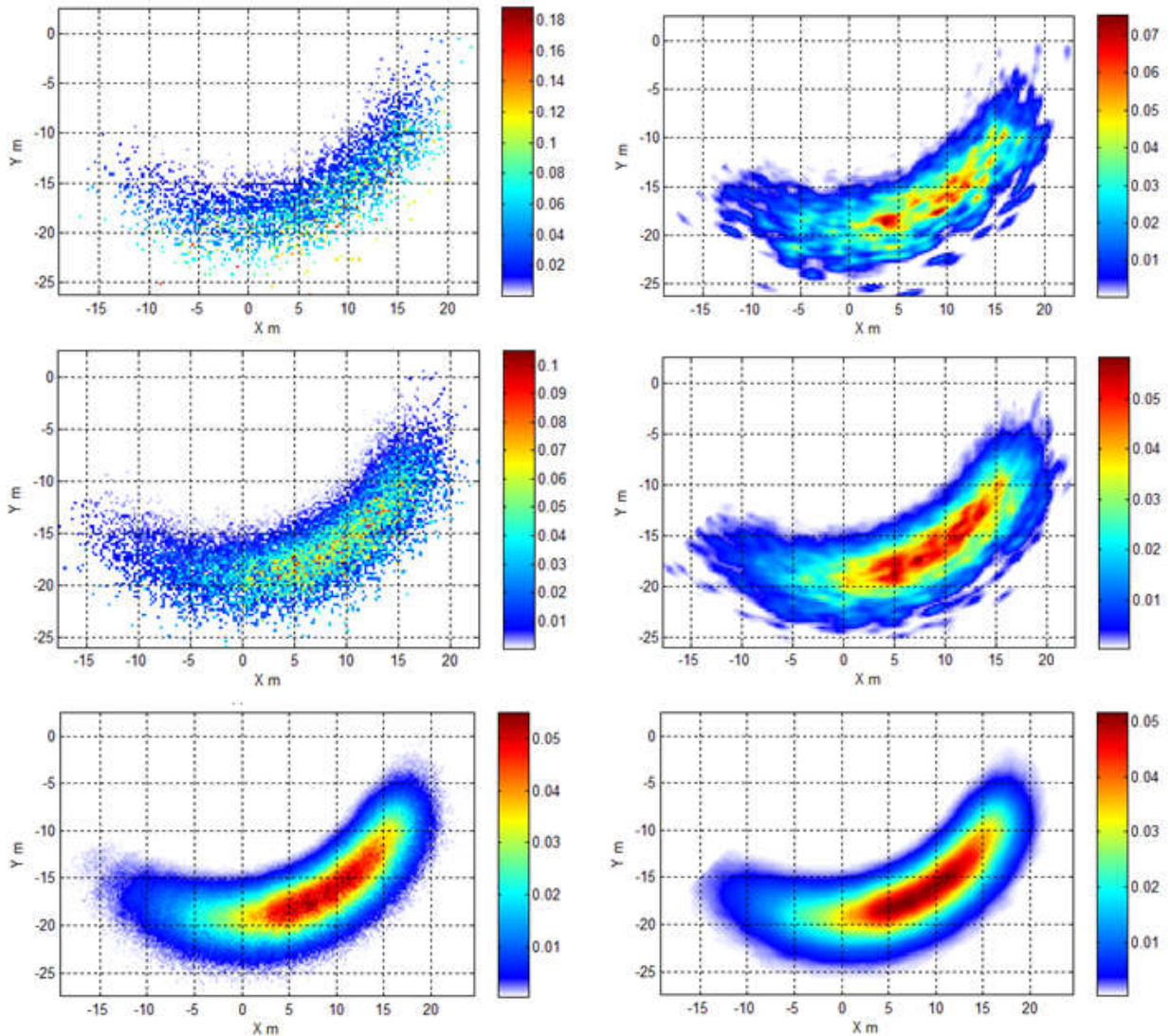
45 The 2D-representation of the spread pattern deposition was obtained by considering a grid
46 with a sampling interval $\Delta w_{grid} = 0.25$ m and $\Delta l_{grid} = 0.25$ m in the transverse and longitudinal
47 directions. Depending on the granule coordinates, the granules located in each grid cell were
48 identified and the sum of their masses was affected to the corresponding cell. This matrix was
49 the raw Cartesian representation of the spread pattern deposition.

1 As the experimental measurement device (CEMIB) was a rotating system, and as the
2 processing of the polar data included some interpolation and regularization steps, it was
3 difficult to compare visually the raw Cartesian representation of the simulated spread pattern
4 with the interpolated experimental measurement (especially for low fertiliser amount).
5 Thus, the raw Cartesian representations of the simulated spread pattern had been sampled in a
6 polar coordinate system, regularized by a Gaussian filter and then re-interpolated into a
7 Cartesian coordinate system to simulate the effect of the Cemib acquisition and data
8 processing. For three different amount of fertiliser, Fig. 7 shows the raw Cartesian
9 representation of the simulated spread pattern deposition and its representation when
10 interpolations are applied in an intermediate polar system.

11 Fig. 7 shows that the local variability increases inside the spread pattern when the fertiliser
12 amount decreases. This corresponds to the well-known random variability observed in CV
13 measurement from run to run. Moreover, when the fertiliser amount is 0.45 kg the
14 representation is in good accordance with the reference spread pattern (Fig. 2) measured with
15 the rotating test bench (when the same fertiliser amount was collected). A better comparison
16 would have been obtained by modeling the rotating acquisition system, but this was out of
17 scope of this paper.

18 When the fertiliser amount is very high (i.e. 50 kg), the relative local variability inside the
19 spread pattern is reduced. Then, the representations of the spread patterns are similar whatever
20 the use of intermediate steps in a polar system or not.

21

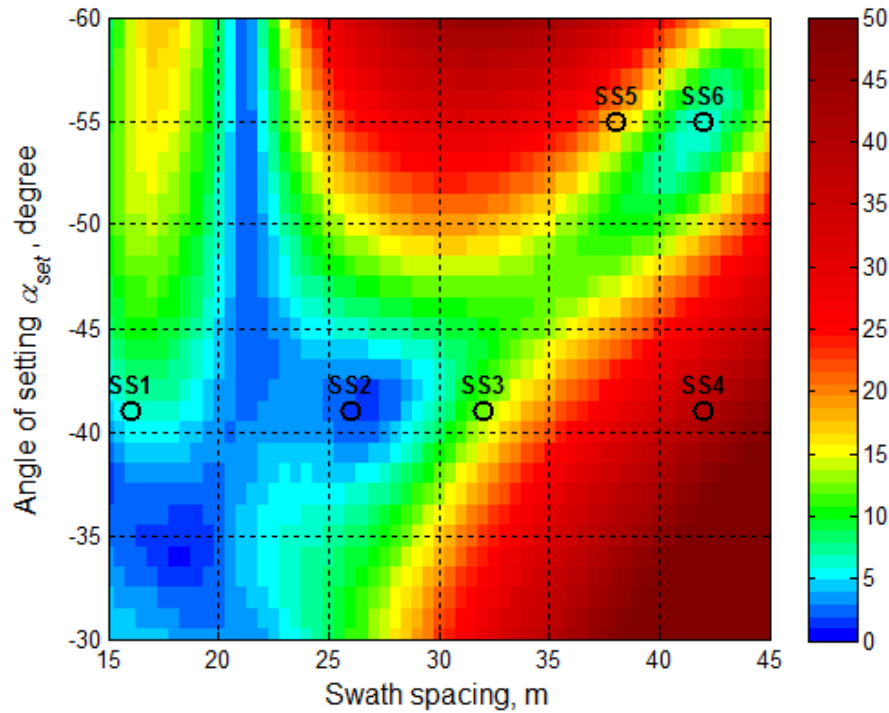


1
 2 Fig. 7 - Simulated spread patterns for three fertiliser amounts: 0.1 kg, 0.45 kg, 50 kg (from top
 3 to bottom) and two kind of representations: raw Cartesian representation of the simulated
 4 spread pattern (left) and after sampling and interpolating in a polar coordinate system (right)
 5 to reflect CEMIB data processing.
 6

7 3.2 Setting map of the virtual spreader

8
 9 A set of simulations were performed to draw the setting map of the virtual spreader. Thus, the
 10 spread pattern was computed by considering 10^6 particles (i.e. a total mass of approximately
 11 26.8 kg) ejected by each disc. The value of the setting angle was from -30° to -60° , and for
 12 each value the transverse CV was computed for a set of swath spacing (from 15 to 45 m). The
 13 size of the virtual collection trays was 0.5×0.5 m each.

14 Figure 8 shows the setting map deduced from the simulations. This map represents the CV
 15 value obtained with the virtual spreader with respect to setting angle and swath spacing. Since
 16 all the CV values were computed for a very high number of particles, these values reflect the
 17 geometry qualities or defects of the spread patterns related to the swath spacing and do not
 18 take into account other transverse variabilities that occur for lower application rates. This CV
 19 value is an estimation of CV_{geom} which is only due to the geometrical shape of the spread
 20 pattern (for a specified swath spacing) regardless of the application rate. CV_{geom} is the value of
 21 CV that would be reached if the application rate tended to infinity.



1
2 Fig. 8 - Setting map of the virtual spreader providing the value of the CV (expressed in
3 percentage) with respect to the setting angle and the swath spacing when the spread pattern is
4 computed for a very high number of fertiliser granules. The color scale corresponds the value
5 of the CV. Six specific spreading situations SS1 to SS6 are marked on the setting map (black
6 circle).

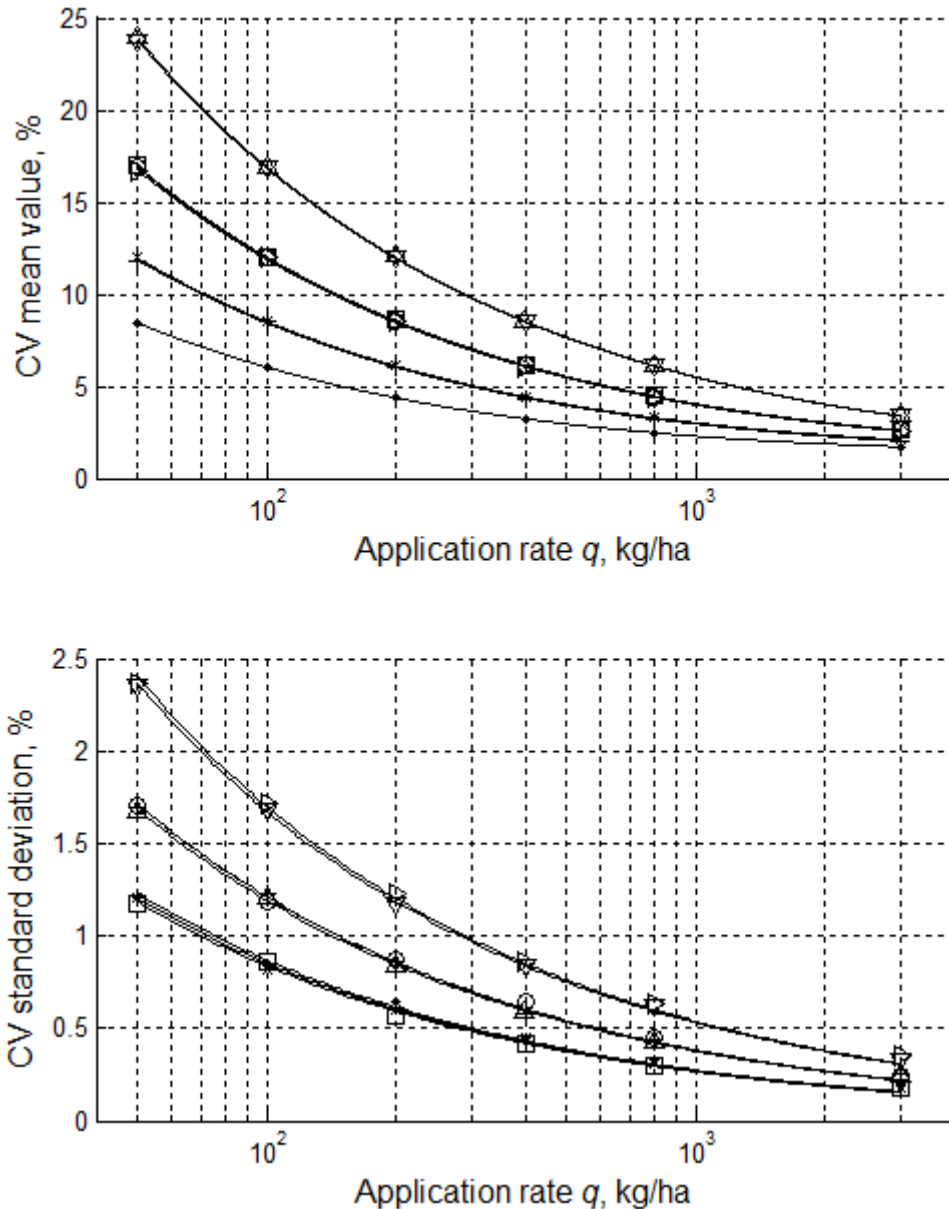
7 8 3.3 Influence of application rate and collection tray size on the CV value 9

10 Simulations have been performed to investigate the effects of the application rate q and the
11 collection tray size on CV measurements. For the simulations, the sizes of the collection trays
12 (length \times width) were: 1 \times 1 m, 1 \times 0.5 m, 1 \times 0.25 m, 0.5 \times 1 m, 0.5 \times 0.5 m, 0.5 \times 0.25 m, 0.25 \times 1
13 m, and 0.25 \times 0.5 m. The application rates were: 50, 100, 200, 400, 800, 3000 kg/ha and for
14 each rate the number of replication runs was respectively 2000, 1000, 500, 500, 400, and 200.
15 The simulations have been computed for six spreading situations (SS1 to SS6) located on the
16 setting map (Fig. 8). Conditions SS1 to SS4 correspond to a setting angle of -41° and swath
17 spacing of respectively 16, 26, 32 and 42 m. Conditions SS5 and SS6 correspond to a setting
18 angle of -55° and swath spacing of respectively 36 and 42 m. These situations have been
19 chosen to illustrate various setting conditions: optimal settings and swath spacing (SS2 and
20 SS6) and inadequate settings or swath spacing.

21 In the case of the situation SS2, Fig. 9 demonstrates that the mean value μ_{CV} and the standard
22 deviation σ_{CV} of the CV increase when the application rate decreases. The curves also show
23 that μ_{CV} and σ_{CV} depend on the size of the collection trays. The mean value μ_{CV} increases
24 when the surface of the collection trays decreases, while the standard deviation σ_{CV} increases
25 when the length of the collection trays decreases.

26 Concerning μ_{CV} , as shown in Fig. 9, it appears that the values are very similar when they are
27 deduced from simulations computed with the same tray surface. Comparing the results
28 obtained for the six spreading situations (SS1 to SS6) at the six application rates, the
29 maximum difference observed on the CV values is 0.36 % for the following tray dimensions
30 1 \times 0.25 m, 0.5 \times 0.5 m, and 0.25 \times 1 m (this maximum difference is obtained for SS4 at 200

1 kg/ha). For the dimensions 1×0.5 m and 0.5×1 m, the maximum difference is 0.24 %
 2 (obtained for SS4 at 3000 kg/ha). For the dimensions 0.5×0.25 m and 0.25×0.5 m, the
 3 maximum difference is 0.23 % (for SS1 at 50 kg/ha). These differences are very low
 4 regarding the traditional range of CV values encountered in practice or regarding μ_{CV} values
 5 encountered here for spreading situations and all application rates (from 1.7 % to 46.3 %).
 6 Furthermore, considering one spreading situation, the mean values of the CV obtained for all
 7 tray size tend to converge.
 8



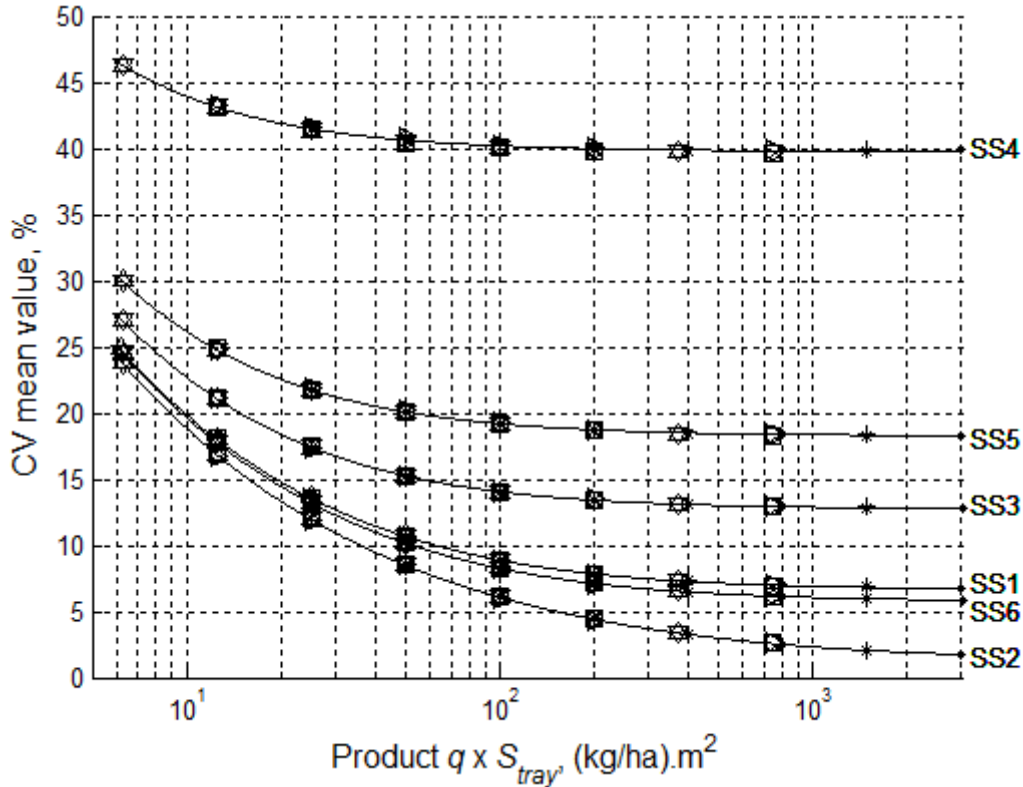
9
 10
 11 Fig. 9 - Mean value (top) and standard deviation (bottom) of the CV values (in %) with
 12 respect to application rate for the spreading situation SS2 and for 8 sizes (length x width) of
 13 collecting trays (• 1×1 m, □ 1×0.25 m, × 1×0.5 m, + 0.5×1 m, ○ 0.5×0.5 m, △ 0.5×0.25 m,
 14 ▷ 0.25×1 m, ▽ 0.25×0.5 m).
 15

16 All these observations lead to consider that the mean value of the CV depends on two
 17 components. One component reflects the spreading situation depending on the setting and on

1 the swath spacing. This component is expressed by the constant value to which μ_{CV} tends for
 2 high application rates. The second component reflects the influence of the application rate
 3 and, more precisely, the influence of the mass collected in trays (depending on the rate and
 4 the tray surface). Consequently, the expression of the mean value of the CV is proposed as a
 5 function of q and S_{tray} as follows:

$$6 \quad \mu_{CV} = \sqrt{\frac{a}{q \times S_{tray}} + b^2} \quad (21)$$

7 where q is expressed in kg/ha, S_{tray} is expressed in m^2 , a and b are two coefficients.
 8 This relationship is used as a regression model to fit the data obtained for the six studied
 9 spreading situations (SS1 to SS6). Figure 10 presents the mean value μ_{CV} with respect to the
 10 product of the application rate by the collection tray surface ($q \times S_{tray}$). Table 1 shows the
 11 values of the parameters a , b and the correlation coefficient resulting from the use of Eq. (21)
 12 to fit the data. The regression curves are drawn on Fig. 10. The values of the correlation
 13 coefficient r demonstrate that Eq. (21) accurately describes the relationship between μ_{CV} , q
 14 and S_{tray} . The lowest value of correlation coefficients is obtained for SS4 but is still higher
 15 than 0.996.



16
 17 Fig. 10 – Mean value of the CV obtained for various spreading situations (SS1 to SS6) when
 18 it is measured with various size of collection trays, with respect to the product of the
 19 application rate by the collection tray surface ($q \times S_{tray}$). The symbols correspond to the size
 20 of the collection trays: • 1x1 m, □ 1x0.25 m, × 1x0.5 m, + 0.5x1 m, ○ 0.5x0.5 m, △
 21 0.5x0.25 m, ▷ 0.25x1 m, ▽ 0.25x0.5 m.

22

1
2
3
4
5
6
7
8
9
10
11
12
13
14
15
16
17
18
19
20
21
22
23
24
25
26
27
28
29
30
31
32
33
34
35
36

Table 1 – Parameters (a , b) and Pearson correlation coefficient (r) of the regression model used to fit CV mean values (expressed in %) according to Eq. (21) for various spreading situations.

Spreading situation	a	b	r
SS1	35.1 10^2	6.64	0.9999
SS2	35.4 10^2	1.38	0.9999
SS3	35.4 10^2	12.74	0.9999
SS4	35.0 10^2	39.76	0.9969
SS5	35.2 10^2	18.26	0.9998
SS6	35.4 10^2	5.76	1.0000

Considering Eq. (21), the value of μ_{CV} tends to b when the application rate approaches infinity. Thus, the parameter b corresponds to the CV_{geom} , which depends on the geometrical shape of the spread pattern (for a specified swath spacing) regardless of the application rate. Regarding Table 1, the values of the parameter a are very similar whatever the spreading situation. Some additional simulations shows that this value depends on the particle size distribution of the fertiliser.

Another interesting aspect of the finding expressed in Eq. (21) is that, whatever the setting of the machine, the mean value of the CV is higher than a limit defined by the application rate and the collection tray surface. This limit is as follows:

$$\mu_{CV} \geq \sqrt{\frac{a}{q \times S_{tray}}} \tag{22}$$

This means that trying to set the machine to obtain a CV below this limit does not make sense. Conversely, measuring CV values significantly higher than this value indicates that the setting or the design of the machine could be optimized to improve the spreading quality. Nevertheless, the practical use of this threshold remains dependent on the accuracy of the CV estimation regarding the measurement variability.

Concerning the standard deviation σ_{CV} of the CV, Fig. 9 shows that the values are close when they are deduced from simulations computed with the same collection tray length.

Comparing the results obtained for the six spreading situations (SS1 to SS6) at the six application rates, the maximum difference observed on the standard deviation is 0.25 % for the following tray dimensions 1x1 m, 1x0.25 m, 1x0.5 m. For the dimensions 0.5x1 m, 0.5x0.5 m, 0.5x0.25 m, the maximum difference is 0.19 %. For the dimensions 0.25x1 m, 0.25x0.5 m, the maximum difference is 0.2 %.

For each collection tray size and for each spreading situation, the standard deviation of the CV is well fitted by the following expression:

$$\sigma_{CV} = c(q \times l_{tray})^{-0.5} \tag{23}$$

The range of values of the parameter c and the range of value of correlation coefficients are presented in Table 2, when q is expressed in kg/ha.

1 Table 2 – Range values of parameter (c) and Pearson correlation coefficient (r) of the
 2 regression model used to fit CV standard deviation values according to Eq. (23) for various
 3 spreading situations.

Spreading situation	c	r
SS1	11.55 to 13.57	0.9893 to 0.9976
SS2	8.35 to 8.66	0.9975 to 0.9996
SS3	8.74 to 10.37	0.9914 to 0.9988
SS4	8.78 to 9.08	0.9980 to 0.9999
SS5	8.89 to 10.13	0.9900 to 0.9993
SS6	6.93 to 7.85	0.9905 to 0.9968

4
 5 In the literature, very few studies addressed the problem of the influence of the application
 6 rate or the collection tray size on the CV value. This is due to the difficulty in performing a
 7 high number of replications and in maintaining constant spreading conditions to establish a
 8 unbiased relationship when actual experiments have to be carried out.

9 Since the quality of the spreading results from numerous combined parameters, simulations
 10 afford the possibility of, not only avoiding perturbations (e.g. humidity, wind or fertilizer
 11 property variations) but also analyzing the studied parameter independently from the others.
 12 This is the case in this section, where the effect of the application rate on the CV is studied
 13 without any change in the outlet angle distribution or in the angular mass flow distribution.
 14 This specific study is very difficult to carry out in practice, because the global shape of the
 15 spread pattern can be modified when the feeding flow rate is modified ([Fulton et al., 2001](#))
 16 due to the change in the feeding area on the spinning disc ([Kweon and Grift, 2006](#)), or in the
 17 vane loading ([Villette et al., 2012](#)).

18
 19 [Parish and de Visser \(1989\)](#) suggested that given a collection tray width w_1 , and a resulting
 20 coefficient of variation CV_1 , a collection tray width of w_2 will result in a new coefficient of
 21 variation CV_2 , related to CV_1 as follows:

$$22 \quad \frac{CV_2}{CV_1} = \sqrt{\frac{w_1}{w_2}} \quad (24)$$

23 The length of the collection tray was implicitly the same for the two kinds of trays. The
 24 authors underlined that, because of variability, this equation should be effective in dealing
 25 with averages of multiple tests.

26 Using Eq.(21), the ratio of the mean value of CV_2 on the mean value of CV_1 is as follows:

$$27 \quad \frac{\mu_{CV_2}}{\mu_{CV_1}} = \sqrt{\frac{a \times q^{-1} \times (l \times w_2)^{-1} + CV_{geom2}^2}{a \times q^{-1} \times (l \times w_1)^{-1} + CV_{geom1}^2}} \quad (25)$$

28 where l is the length of the collection trays (which is the same for the collection trays used to
 29 measure CV_1 and CV_2).

30 It appears that the relationship between CV_2 and CV_1 is more complex than the one suggested
 31 by [Parish and de Visser \(1989\)](#) and that Eq.(24) is not correct when the geometrical
 32 component of the CV (CV_{geom}) is not null. Nevertheless, in the case of a good quality
 33 spreading, CV_{geom1} and CV_{geom2} are low and are negligible compared to the component related
 34 to the effect of the application rate. In the case of a good quality spreading, Eq.(25) yields:

$$35 \quad \frac{\mu_{CV_2}}{\mu_{CV_1}} = \sqrt{\frac{w_2^{-1}}{w_1^{-1}}} = \sqrt{\frac{w_1}{w_2}} \quad (26)$$

36 This demonstrates that the relationship proposed by [Parish and de Visser \(1989\)](#) is a correct
 37 approximation only when the setting of the machine is very good, or when the CV value is
 38 widely due to the effect of the application rate (low application rate).

1
2 Simulation findings demonstrate the variability in CV measurement (i.e. σ_{CV}) decreases with
3 the application rate and the length of the collection trays used for the measurement. These
4 results are in perfect accordance with recommendations of [Jones et al. \(2008\)](#) who concluded
5 that multiple rows of trays, multiple passes and long trays can reduce experimental variability
6 and improve the accuracy of bout width calculation. It is worth noting that doubling the
7 number of passes corresponds to doubling the apparent application rate collected by the tray.
8 Concerning the collection trays used for transverse tests, the European Standard specified in
9 [EN 13739-2 \(2011\)](#) recommends the size (length x width) of 0.5×0.5 m but also permits
10 1×0.25 m. The simulation findings confirmed that the mean value expected for the CV is the
11 same when these two collection tray sizes are used. Nevertheless, simulations demonstrates
12 these two collection devices are not equivalent regarding the variability in CV measurement.
13 Thus, the variability is reduced when the size of 1×0.25 m is used and the confidence in bout
14 width calculation is improved. This illustrates that simulations would be of practical interest
15 when standard revision process are launched.

16 17 **3.4 Influence of the test method on the CV value**

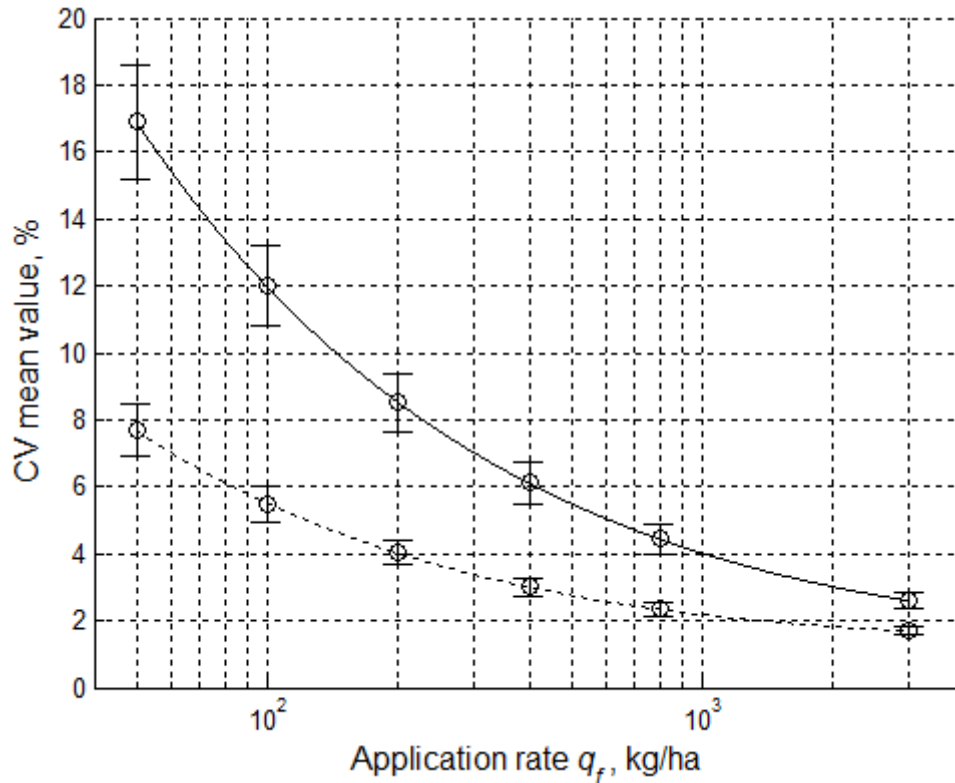
18
19 Simulations had been carried out to compare the values of CV when they were obtained
20 following two different measurement methods. The first method was a simple “in-field”
21 measurement consisting in measuring the CV when the machine was driven at the forward
22 speed of 10 km/h and was set to apply the in-field target rate q_f . The second method was a
23 “standard test” performed following the European Standard specified in [EN 13739-2 \(2011\)](#).
24 In this standard test, the machine was driven at 4 km/h, the number of runs for each
25 measurement was two, and the flow adjustment using 4 km/h was set to correspond to the
26 flow rate obtained at a forward driving speed of 10 km/h. Thus, in practice, the application
27 rate used in the simulation program for the virtual standard test was:

$$28 \quad q = \frac{10}{4} q_f \quad (27)$$

29 Following the European Standard, two replications were done for each virtual standard test
30 before computing the corresponding CV. Moreover, the mirror image of the transverse
31 distribution of the central pass was used to compute the overlapped distribution with the
32 adjacent passes on the swath spacing. In contrast, concerning the virtual “in-field”
33 measurement, no replication is done before computing the corresponding CV and the
34 transverse distributions for each pass were completely independent (i.e. no mirror image was
35 used). For both test procedures, the same transverse line of collection trays was used. The size
36 of these virtual trays was 0.5×0.5 m.

37 For the spreading situation SS2, Fig. 11 presents the mean value and error bar (twice the
38 standard deviation) of the CV with respect to the application rate. The mean value and the
39 standard deviation of the CV decrease with the application rate. The figure also shows that the
40 CV is lower when it is measured with the standard procedure than when it is measured with
41 the simple in-field test. Moreover, the standard deviation is lower when it is measured
42 following the standard procedure (the standard deviation is approximately divided by 2).
43 These results illustrate that the use of the standard test reduce the variability on the
44 measurement of the CV. Nevertheless, the standard test underestimates the value of the CV
45 with respect to the value that should be obtained in field by considering the actual target
46 application rate (i.e. with the actual application rate at the actual forward speed and without
47 any replication). In this example, the “in-field” CV is at least twice the “standard” CV when
48 the application rate is lower than 490 kg/ha.

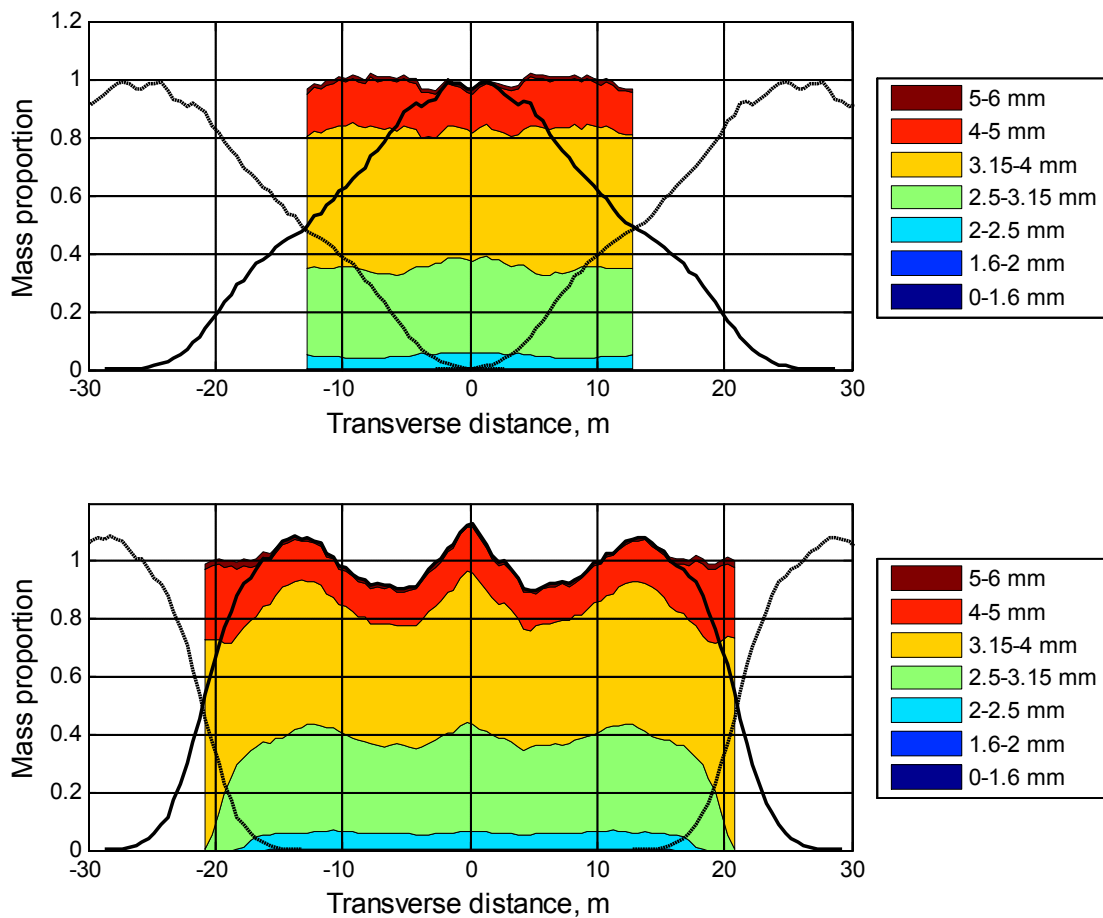
1 The differences observed here only result from the measurement procedure since no
 2 additional perturbation (i.e. wind, ground topography, ground irregularity, guidance error...)
 3 was taken into account for the “in field” measurements. Thus, the “in-field” CV defined in
 4 this section should not be confused with the “field CV” defined by [Lawrence and Yule](#)
 5 ([2007](#)).



6
 7 Fig. 11 – Mean value and error bar (twice the standard deviation) of the CV with respect to
 8 the application rate for the spreading situation SS2. Simulations are performed with collection
 9 trays of 0.5×0.5 m for virtual “in-field” measurements (continuous line) and for virtual
 10 “standard” measurements (dotted line).

12 3.5 Influence of granule size and drag coefficient

13
 14 One particularity of the spread pattern simulations described in this article was that each
 15 fertilizer granule was tracked during the whole virtual spreading process. Consequently, at the
 16 end of the process, when all granules lied on the ground, the location and the diameter of each
 17 granule were perfectly known. Thus, simulations were used to study how fertiliser particles
 18 contribute to the transverse distribution in relation to their diameters. Figure 12 presents the
 19 transverse distributions of the fertilizer sieve fractions for two spreading situations: SS2 and
 20 SS5. For each situation, simulations have been performed with 10^6 fertiliser granules per disc.
 21 The size of the virtual collection trays was 0.5×0.5 m. In the case of situation SS2, the
 22 proportions of each diameter class are approximately kept constant on all the working width
 23 (26 m) and correspond to the particle size analysis presented in Fig. 12. In this situation, the
 24 transverse distribution has a triangular shape before overlapping and adjacent passes overlap
 25 on a large part of the working width. In contrast, in the case of situation SS6, the proportions
 26 of diameter classes are modified at the extremities of the working width with small diameter
 27 vanishing. In this last situation, the swath spacing is 42 m, the transverse distribution has a
 28 trapezoidal shape before overlapping and adjacent passes overlap only on a low part of the
 29 working width. Thus, the overlapping area only concerns the external part of the spread
 30 pattern and the landing points of biggest granules.

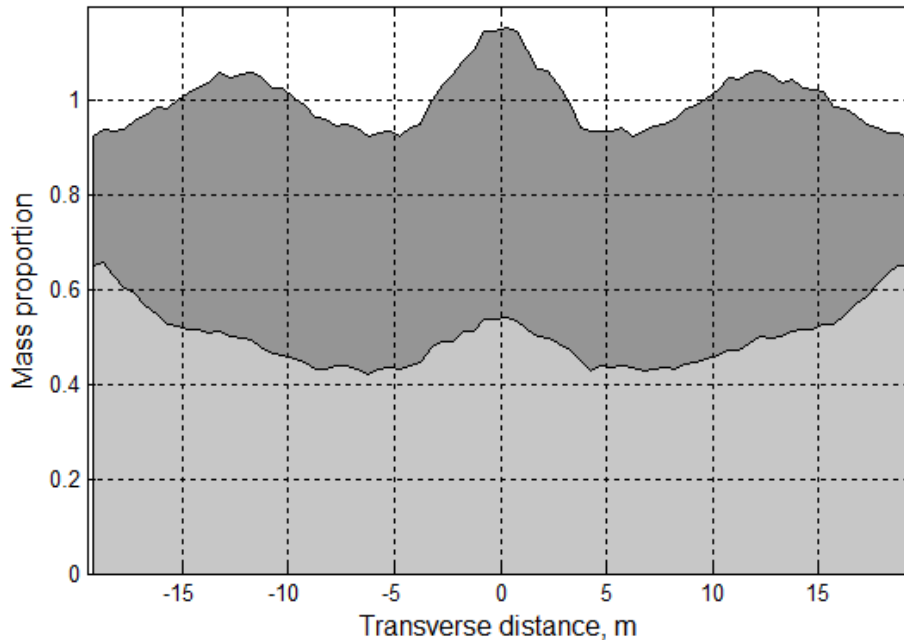


1
2 Fig. 12 – Overlapped transverse distribution of fertiliser diameter classes on the working
3 width, in the case of two spreading situations: SS2 (top) for a spacing width of 26 m and SS6
4 (bottom) for a spacing width of 42 m. The transverse mass distributions are superposed for the
5 central pass (continuous black line) and adjacent passes (dashed black line).
6

7 In the case of situation SS6, the same rate (i.e. same mass per surface unit) is applied locally
8 at 2.5 m and 21 m from the centerline of the virtual spreader, but the number of granules per
9 surface unit is not the same. For the same application rate, the number of granules decrease
10 when their sizes increase. Consequently, this affects the spatial variability of the fertiliser
11 supply at very small scales. A further characterization of this effect is worth of studying but is
12 out of scope for this article.

13 The study of spreading segregation is also of particular interest for blended fertilisers. The
14 HCSM is an interesting tool to investigate how ballistic segregation affects the spatial
15 distribution of each fertiliser components. To illustrate this aspect, a simulation was
16 performed by considering two fertiliser components and one spreading situation. The first
17 fertiliser component corresponded to ammonium nitrate whose characteristics had been
18 described and used in the previous sections. The second fertiliser component corresponded to
19 a fictive material, which only differ by the drag coefficient set at 0.60 (instead of 0.47 for the
20 first component). This C_d value was the one used by [Grafton et al. \(2015\)](#). Considering that
21 the two fertiliser components were in the same weight proportion, the simulation was carried
22 out for a setting angle of -54° and a swath spacing of 39 m. In these spreading conditions, Fig.
23 13 shows the transverse distribution of the blended fertilisers and of each component. The CV
24 computed for the blended fertilisers was 6.1 %. Nevertheless, the CV values were at least

1 twice when each fertiliser component was considered independently. Thus, the CV reached
2 12.5% for the first component and 17.1% for the second one. This illustrates that the
3 measurement of the CV for blended fertilisers (i.e. measured without differencing the
4 components) does not systematically provide a good assessment of the spatial chemical
5 variability.



6
7 Fig 13. Overlapped transverse distribution of blended fertilisers that only differ in their
8 respective drag coefficient: 0.47 (in light grey) and 0.60 in (in dark grey).
9

10 The benefit of this approach is that results are not limited to comparison of the ballistic
11 lengths of individual particles in contrast with works of [Antille et al. \(2015\)](#) or [Grafton et al.](#)
12 [\(2015\)](#). The present approach considers the two-dimensional spread pattern so that the
13 transverse distribution is computed taking into account the overlapping of adjacent passes.
14

15 This section put the emphasis on the interest of HCSM to investigate the impact of fertiliser
16 properties on the transverse distribution. The accurate study of a specific blended fertiliser
17 would require to characterize the mechanical behavior of the mixture on the spinning disc to
18 provide the horizontal and vertical outlet angle distributions and the angular mass flow
19 distribution (as described in section 2.2). It would also required to characterize the properties
20 of each fertiliser components in terms of specific density, diameter distribution and drag
21 coefficient (as described in section 2.3). Using these input parameters, the HCSM would be an
22 efficient and low cost strategy to study the behaviour of blended fertilisers and provide
23 recommendations on swath spacing.
24

25 4. Conclusion

26
27 To simulate fertiliser spread pattern depositions, a hybrid model was proposed. This approach
28 combined the use of theoretical motion equations and experimental results. The experimental
29 data were used to adjust few constant parameters and to provide the statistical distributions of
30 other input parameters. This ensured the realistic nature of fertiliser mechanical behaviours
31 and spread pattern simulations. The particularity of the hybrid model was the use of
32 successive random selections to compute the spread pattern deposition of virtual particles
33 whose size and motion parameters respected experimental statistical distributions. This Monte

1 Carlo process took into account the variability of input parameters and made possible the use
2 of simulation replications to access to statistical characteristics of the output variables.
3 Simulation results showed the Hybrid Centrifugal Spreading Model was worth of interest to
4 study information that was difficult or impossible to access with actual experiments. In
5 particular, results demonstrated the transverse CV not only depended on the spreader setting
6 and the swath spacing but also increased when the application rate decreased. The CV value
7 also increased when the collection tray surface decreased. A mathematical relationship had
8 been derived from simulation results to describe these influences. The study also
9 demonstrated the variability of CV measurements increased when the application rate or the
10 collection tray length decreased. Differences observed in the CV value, when it was measured
11 in field or following the standard specified in EN 13739-2, were highlighted.
12 An insight into the distribution of the fertiliser particles related to their diameter or their drag
13 coefficient showed the Hybrid Centrifugal Spreading Model will be a powerful tool to analyse
14 further the impact of fertiliser ballistic properties on the spread pattern.
15 More generally, the model and the associated Monte Carlo simulations open up the possibility
16 of carrying out virtual and numerical experiments to avoid cumbersome experimental tasks
17 for numerous research or development activities. For instance, this will be of particular
18 interest in: studying the effects of perturbing factors such as wind; providing
19 recommendations concerning the use of blended fertilisers for a selected swath spacing;
20 comparing different test methods to assess the transverse distribution or the spread pattern
21 (especially to design simplified tests); assessing the accuracy of test methods (especially in
22 defining the optimal swath width); or defining the probability of obtaining a selected range of
23 application rate for a selected spatial scale defined by agronomical criteria.
24
25

26 5. References

- 28 Antille, D.L., Gallar-Redondo, L., Godwin, R.J., 2013. Determining the particle size range of
29 organomineral fertilisers based on the spreading characteristics of the material, ASABE
30 Annual International Meeting, Kansas City, Missouri, July 21-July 24, 2013. American
31 Society of Agricultural and Biological Engineers, p. 18.
- 32 Antille, D.L., Gallar, L., Miller, P., Godwin, R., 2015. An investigation into the fertilizer
33 particle dynamics off-the-disc. *Applied Engineering in Agriculture* 31, 49-60.
- 34 Aphale, A., Bolander, N., Park, J., Shaw, L., Svec, J., Wassgren, C., 2003. Granular fertiliser
35 particle dynamics on and off a spinner spreader. *Biosystems Engineering* 85, 319-329.
- 36 ASAE Standards S341.2, 1999. Procedure for measuring distribution uniformity and
37 calibrating granular broadcast spreaders, ASAE, St. Joseph, Michigan, USA.
- 38 Australian Fertiliser Services Association, 2001. Accu-Spread - Code of practice for
39 spreading, Glenthompson.
- 40 Bradley, M., Farnish, R., 2005. Segregation of Blended Fertiliser During Spreading: The
41 Effect of Differences in Ballistic Properties, International Fertiliser Society. IFS, United
42 Kingdom.
- 43 Casas, G., Mukherjee, D., Celigueta, M.A., Zohdi, T.I., Onate, E., 2015. A modular,
44 partitioned, discrete element framework for industrial grain distribution systems with
45 rotating machinery. *Computational Particle Mechanics*, 1-18.
- 46 Coetzee, C.J., Lombard, S.G., 2011. Discrete element method modelling of a centrifugal
47 fertiliser spreader. *Biosystems Engineering* 109, 308-325.
- 48 Cool, S., Vangeyte, J., van Damme, J., Sonck, B., Pieters, J., van de Gucht, T., Mertens, K.,
49 2015. Comparison of different spread pattern determination techniques, *Precision
50 agriculture'15*. Wageningen Academic Publishers, p. 146.

- 1 Cunningham, F.M., 1963. Performance characteristics of bulk spreaders for granular fertilizer.
2 Transactions of the ASAE 6, 108-0114.
- 3 Cunningham, F.M., Chao, E.Y., 1967. Design relationships for centrifugal fertilizer
4 distributors. Transactions of the ASAE 10, 91-0095.
- 5 EN 13739-2, 2003. Agricultural machinery - Solid fertilizer broadcasters and full width
6 distributors - Environmental protection - Part 2: Test methods., European Committee for
7 Standardisation.
- 8 EN 13739-2, 2011. Agricultural machinery - Solid fertilizer broadcasters and full width
9 distributors - Environmental protection - Part 2: Test methods, European Committee for
10 Standardization, Bruxelles.
- 11 Fulton, J., Shearer, S., Chabra, G., Higgins, S., 2001. Performance assessment and model
12 development of a variable-rate, spinner-disc fertilizer applicator. Transactions of the
13 ASAE 44, 1071.
- 14 Gomez-Gil, J., de-Lozar-Escudero, A., Navas-Gracia, L., Ruiz-Ruiz, G., 2009. Analytical
15 estimation of optimal operation variables of a centrifugal fertilizer distributor, using the
16 gradient method on multiple seeds. *Agrociencia (Montecillo)* 43, 497-509.
- 17 Grafton, M., Yule, I., Robertson, B., Chok, S., Manning, M., 2015. Ballistic Modeling and
18 Pattern Testing to Prevent Separation of New Zealand Fertilizer Products. *Applied
19 Engineering in Agriculture* 31.
- 20 Griffis, C., Ritter, D., Matthews, E., 1983. Simulation of rotary spreader distribution patterns.
21 Transactions of the ASAE 26, 33-37.
- 22 Grift, T., Hofstee, J., 2002. Testing an online spread pattern determination sensor on a
23 broadcast fertilizer spreader. Transactions of the ASAE 45, 561-570.
- 24 Grift, T., Kweon, G., Hofstee, J., Piron, E., Villette, S., 2006. Dynamic Friction Coefficient
25 Measurement of Granular Fertiliser Particles. *Biosystems Engineering* 95, 507-515.
- 26 Hoffmeister, G., Watkins, S., Silverberg, J., 1964. Fertilizer Consistency, Bulk Blending of
27 Fertilizer Material: Effect of Size, Shape, and Density on Segregation. *Journal of
28 Agricultural and Food Chemistry* 12, 64-69.
- 29 Hofstee, J.W., 1995. Handling and Spreading of Fertilizers: Part 5, The Spinning Disc Type
30 Fertilizer Spreader. *Journal of Agricultural Engineering Research* 62, 143-162.
- 31 Horrell, R., Metherell, A., Ford, S., Doscher, C., 1999. Fertiliser evenness-losses and costs: a
32 study on the economic benefits of uniform applications of fertiliser, New Zealand
33 Grassland Association Conference, pp. 215-220.
- 34 Inns, F., Reece, A., 1962. The theory of the centrifugal distributor II: Motion on the disc, off-
35 centre feed. *Journal of Agricultural Engineering Research* 7, 345-353.
- 36 ISO Standard 5690/1, 1985. Equipment for Distributing Fertilizers: Test Methods, part 1: Full
37 width fertilizer distributors, International Organization for Standardization, Genève.
- 38 Jensen, D., Pesek, J., 1962. Inefficiency of fertilizer use resulting from nonuniform spatial
39 distribution: II. Yield losses under selected distribution patterns. *Soil Science Society of
40 America Journal* 26, 174-178.
- 41 Jones, J.R., Lawrence, H.G., Yule, I.J., 2008. A statistical comparison of international
42 fertiliser spreader test methods - Confidence in bout width calculations. *Powder
43 Technology* 184, 337-351.
- 44 Kweon, G., Grift, T.E., 2006. Feed Gate Adaptation of a Spinner Spreader for Uniformity
45 Control. *Biosystems Engineering* 95, 19-34.
- 46 Lawrence, H., Yule, I., 2007. Estimation of the in-field variation in fertiliser application. *New
47 Zealand Journal of Agricultural Research* 50, 25-32.
- 48 Mennel, R., Reece, A., 1963. The theory of the centrifugal distributor III: Particle trajectories.
49 *Journal of Agricultural Engineering Research* 7, 78-84.

- 1 Miller, P.C., Audsley, E., Richards, I.R., 2009. Costs and effects of uneven spreading of
2 nitrogen fertilisers, Conference of the International Fertiliser Society, Cambridge, UK,
3 10th December 2009. International Fertiliser Society, pp. 1-24.
- 4 Miserque, O., Pirard, E., 2004. Segregation of the bulk blend fertilizers. *Chemometrics and*
5 *intelligent laboratory systems* 74, 215-224.
- 6 New Zealand Fertiliser Quality Council, 2015. Spreadmark code of practice, Wellington New
7 Zealand: Online publication. Retrieved from <http://www.fertqual.co.nz>.
- 8 Olieslagers, R., 1997. Fertilizer distribution modelling for centrifugal spreader design. PhD
9 Thesis, nr. 341. aan de faculteit der landbouwwetenschappen, K. U. Leuven, Belgium.
- 10 Olieslagers, R., Ramon, H., De Baerdemaeker, J., 1996. Calculation of Fertilizer Distribution
11 Patterns from a Spinning Disc Spreader by means of a Simulation Model. *Journal of*
12 *Agricultural Engineering Research* 63, 137-152.
- 13 Parish, R., 1986. Comparison of spreader pattern evaluation methods. *Applied Engineering in*
14 *Agriculture* 2, 89-93.
- 15 Parish, R., Chaney, P., Fuller, D., 1987. Comparison of laboratory methods of spreader
16 pattern evaluation with agronomic response. *Applied Engineering in Agriculture* 3, 237-
17 240.
- 18 Parish, R., de Visser, P., 1989. Technical Notes: Experimental Verification of the Effect of
19 Collection Pan Width on Apparent Spreader Pattern. *Applied Engineering in*
20 *Agriculture* 5, 163-164.
- 21 Patterson, D., Reece, A., 1962. The theory of the centrifugal distributor. I: Motion on the disc,
22 near-centre feed. *Journal of Agricultural Engineering Research* 7, 232-240.
- 23 Pettersen, J., Svendsen, J., Øvland, S., 1991. A method of studying the influence of fertilizer
24 particle size on the distribution from a twin-disc spreader. *Journal of agricultural*
25 *engineering research* 50, 291-303.
- 26 Piron, E., Miclet, D., 2005. Centrifugal fertiliser spreaders: a new method for their evaluation
27 and testing, Conference of the International Fertiliser Society, York, United Kingdom.
28 The International Fertiliser Society, p. 22p.
- 29 Piron, E., Miclet, D., Villette, S., 2010. CEMIB: an innovative bench for spreader eco-design,
30 AgEng 2010, International Conference on Agricultural Engineering, Clermont-Ferrand,
31 France, p. 9 p.
- 32 Pitt, R., Farmer, G., Walker, L., 1982. Approximating equations for rotary distributor spread
33 patterns. *Transactions of the ASAE* 25, 1544-1552.
- 34 Reumers, J., Tijskens, E., Ramon, H., 2003. Experimental Characterisation of the Tangential
35 and Cylindrical Fertiliser Distribution Pattern from a Spinning Disc: A Parameter
36 Study. *Biosystems Engineering* 86, 327-337.
- 37 Richards, I.R., Hobson, R.D., 2013. Method of calculating effects of uneven spreading of
38 fertiliser nitrogen. *International Fertiliser Society Proc. No. 734*.
- 39 Sogaard, H.T., Kierkegaard, P., 1994. Yield reduction resulting from uneven fertilizer
40 distribution. *Transactions of the ASAE* 37, 1749-1752.
- 41 Tijskens, B., van Liedekerke, P., Ramon, H., 2005. Modelling to aid assessment of fertiliser
42 handling and spreading characteristics, Conference of the International Fertiliser
43 Society, York, United Kingdom. The International Fertiliser Society.
- 44 Tissot, S., Miserque, O., Mostade, O., Huyghebaert, B., Destain, J., 2002. Uniformity of N-
45 fertiliser spreading and risk of ground water contamination. *Irrigation and drainage* 51,
46 17-24.
- 47 Tissot, S., Quenon, G., Miserque, O., 1999. Tolérance d'une culture de froment à l'égard de
48 l'hétérogénéité d'épandage des engrais azotés. *Biotechnologie, Agronomie, Société et*
49 *Environnement* 3, 247-252.

- 1 Van Liedekerke, P., Tijsskens, E., Dintwa, E., Anthonis, J., Ramon, H., 2006. A discrete
2 element model for simulation of a spinning disc fertilizer spreader I. Single particle
3 simulations. *Powder Technology* 170, 71-85.
- 4 Van Liedekerke, P., Tijsskens, E., Dintwa, E., Rioual, F., Vangeyte, J., Ramon, H., 2009. DEM
5 simulations of the particle flow on a centrifugal fertilizer spreader. *Powder technology*
6 190, 348-360.
- 7 Villette, S., Piron, E., Cointault, F., Chopinet, B., 2005. Centrifugal Spreading: an Analytical
8 Model for the Motion of Fertiliser Particles on a Spinning Disc. *Biosystems*
9 *Engineering* 92, 157-164.
- 10 Villette, S., Piron, E., Cointault, F., Chopinet, B., 2008. Centrifugal spreading of fertiliser:
11 Deducing three-dimensional velocities from horizontal outlet angles using computer
12 vision. *Biosystems Engineering* 99, 496-507.
- 13 Villette, S., Piron, E., Martin, R., Miclet, D., Jones, G., Paoli, J., Gée, C., 2013. Estimation of
14 two-dimensional fertiliser mass flow distributions by recording granule impacts.
15 *Biosystems Engineering* 115, 463-473.
- 16 Villette, S., Piron, E., Miclet, D., Martin, R., Jones, G., Paoli, J., Gée, C., 2012. How mass
17 flow and rotational speed affect fertiliser centrifugal spreading: Potential interpretation
18 in terms of the amount of fertiliser per vane. *Biosystems Engineering* 111, 133-138.
- 19 Virk, S.S., Mullenix, D.K., Sharda, A., Hall, J.B., Wood, C.W., Fasina, O.O., McDonald,
20 T.P., Pate, G.L., Fulton, J.P., 2013. Case Study: Distribution uniformity of a blended
21 fertilizer applied using a variable-rate spinner disc spreader. *Applied Engineering in*
22 *Agriculture* 29, 627-636.
- 23 Walker, J., Grift, T., Hofstee, J., 1997. Determining effects of fertilizer particle shape on
24 aerodynamic properties. *Transactions of the ASAE* 40, 21-27.
- 25 Yule, I., 2011. The effect of fertilizer particle size on spread distribution. NZ Centre for
26 Precision Agriculture, Massey University, Palmerston North, New Zealand, 1-9.
- 27